CHEMICAL ORDER IN THE HEUSLER ALLOYS $Ni_2Mn_xV_{1-x}Sn$ BY NEUTRON DIFFRACTION

By

© LUC MARTIN, B.Sc. Phys.

A Thesis

Submitted to the School of Graduate Studies

in Partial Fulfilment of the Requirements

for the Degree

Master of Science

McMaster University

March 1982

CHEMICAL ORDER IN $Ni_2Mn_xV_{1-x}Sn$

MASTER OF SCIENCE (1982)

McMASTER UNIVERSITY
Hamilton, Ontario

TITLE: Chemical Order in the Heusler Alloys $Ni_2Mn_xV_{1-x}Sn$ by Neutron Diffraction

AUTHOR: LUC MARTIN, B.Sc. Phys. (Université de Montréal)

SUPERVISOR: Professor C.V. Stager

NUMBER OF PAGES: vii, 74

ABSTRACT

The chemical ordering in samples of Heusler alloys of the series $Ni_2Mn_xV_{1-x}Sn$, where x stands for 1.0, 0.8, and 0.6, has been measured by neutron diffraction. Measurements were performed at room temperature. The samples were long thin single crystals with cross-section less than 1 mm. The samples had been cut by spark erosion from large single crystal boules. Extinction was still present. The data were fitted with a nuclear structure factor, allowing for chemical disorder, based on a model of the crystal structure. They highly order in the $L2_1$ type crystal structure. Slight Mn,V$\longleftrightarrow$Ni disorder was sufficient to explain the data. For x=1.0, (3.5 ± 1.2) at. % disorder between Mn-V and Ni atoms was necessary to obtain the best fit. For x=0.8 the best fit was obtained with no disorder. Disorder was (2.8 ± 0.9) at. % between Mn-V and Ni atoms for the x=0.6 sample. No evidence of any other type of disorder was found.

ACKNOWLEDGMENTS

The completion of this work was made possible by the sustained interest of my supervisor, Dr. C.V. Stager. I sincerely thank him for the guidance I owe him. Many discussions and useful hints were provided by Dr. K.E. Locke, a student colleague, whose friendship was a moral support.

I also wish to thank Mr. J. Couper for his technical assistance. For the typing of the manuscript, I thank Miss D. Laurin.

Finally, I gratefully thank Yolaine, my wife, for her never-fading confidence in seeing the completion of this thesis.

TABLE OF CONTENTS

LIST OF FIGURES

LIST OF TABLES

CHAPTER I

INTRODUCTION

The series of Heusler alloys $Ni_2Mn_xV_{1-x}Sn$ have had their magnetic properties intensively investigated. These alloys, of basic stoichiometric composition Ni_2YSn, where Y can be either occupied by a Mn or V atom, have the $L2_1$ crystal structure. They are all ferromagnetic for large x, Mn carrying all of the magnetization of approximately $4\mu_B$ per manganese atom. It is interesting to note that metallic Mn is antiferromagnetic. It is known that chemical order can perturb the magnetic properties of such alloys. Little data are available from measurements of chemical order in Heusler alloys. The few that do exist are based on polycrystalline samples. Because of the extensive study of this particular series by our group it became necessary to perform such measurements. Chemical order measurements of single crystal samples from this series is the topic of this thesis.

The remainder of this chapter describes Heusler alloys by a brief historical review. Chapter two outlines the theory behind the method of neutron diffraction. The cross-sections for nuclear and magnetic scattering are derived. Topics such as Debye-Waller factor, thermal diffuse scattering, absorption and extinction are discussed. A structure model for $Ni_2Mn_xV_{1-x}Sn$ is proposed and structure factors are calculated for this model. The room temperature

contribution of magnetic scattering to the total scattering is calculated for Ni_2MnSn. The third chapter relates how the crystals were grown, the various experiments that were done and the apparatus involved. Chapter four consists of the neutron diffraction data and results pertaining to the chemical order. Chapter five contains the conclusions of this study. In the appendix are various tables of the results.

F. Heusler (1903) first showed that ferromagnetic materials could be made from normally non-ferromagnetic elements. He alloyed together copper-manganese bronze with tin, aluminum, antimony, bismuth, arsenic or boron to obtain what are now called "Heusler alloys".

Heusler alloys have a metallic lustre and the high conductivity of metals. As well, the structure of Heusler alloys is the one of an ordered compound. Hence they are classified as intermetallic compounds. The common chemical order is X_2YZ, where X stands for transition metal such as Cu, Ni, Pd, or Co; Y is usually Mn; and Z stands for a group IIIB, IVB or VB element such as Al, In, Sb or Sn.

The crystal structure of Heusler alloys was resolved over a period of time. Persson (1928) studied a ferromagnetic alloy, near the composition Cu_2MnAl, by x-rays. No attempt was made to differentiate the Cu atoms from the Mn atoms, this being difficult with x-rays. He concluded that Cu_2MnAl was body-centred cubic (BCC) but with the Al atoms forming a face-centred cubic (FCC) superlattice as in Fe_3Al (Strukturbericht DO_3). Potter (1929) studying Cu_2MnAl arrived at the same conclusion. However, torsion magnetometer results suggested to him that Mn was also distributed on a FCC sublattice. Bradley and

Rogers (1934) were the first to elucidate the complete crystal structure of Heusler alloys and they also showed the prime importance of the structure in the understanding of the magnetic properties. They investigated an alloy near the composition Cu_2MnAl. To differentiate between Cu and Mn, they used 3 different x-ray wavelengths to exploit anomalies in atomic scattering factor near an absorption edge. The crystal structure is the one suggested by Potter, i.e. four interpenetrating FCC sublattices, strukturbericht $L2_1$. For Ni_2MnSn, the Ni atoms occupy the positions (000) and (½½½), the Mn atoms, (¼¼¼), and the Sn atoms, the (3/4 3/4 3/4) sites, as in Figure I-1. To show that crystal structure is more important than chemical composition for the magnetic properties they determined that the crystal chosen experienced an almost complete loss of magnetism when the structure changed with heat treatment. The development of neutron diffraction provided a powerful tool for research in magnetism. Not only accurate determination of magnetic and chemical structure became possible, but also the study of phonons and spin waves permitted the investigation of the nature of the forces involved in a crystal. Bacon (1975) is an excellent reference for the application of neutron diffraction to these problems.

Neutron diffraction studies (Felcher (1963); Webster (1967), (1968), (1971); Bacon (1971)) show that most Heusler alloys containing Mn have a localized magnetic moment at the Mn site of about $4\mu_B$ unless X, in the stoichiometric composition, is cobalt. The mechanism responsible for the coupling of these moments has not been resolved. Ishikawa et al (1974, 1976, 1977) observed a long range oscillatory

Fig. I-1: Structure of Ni_2MnSn

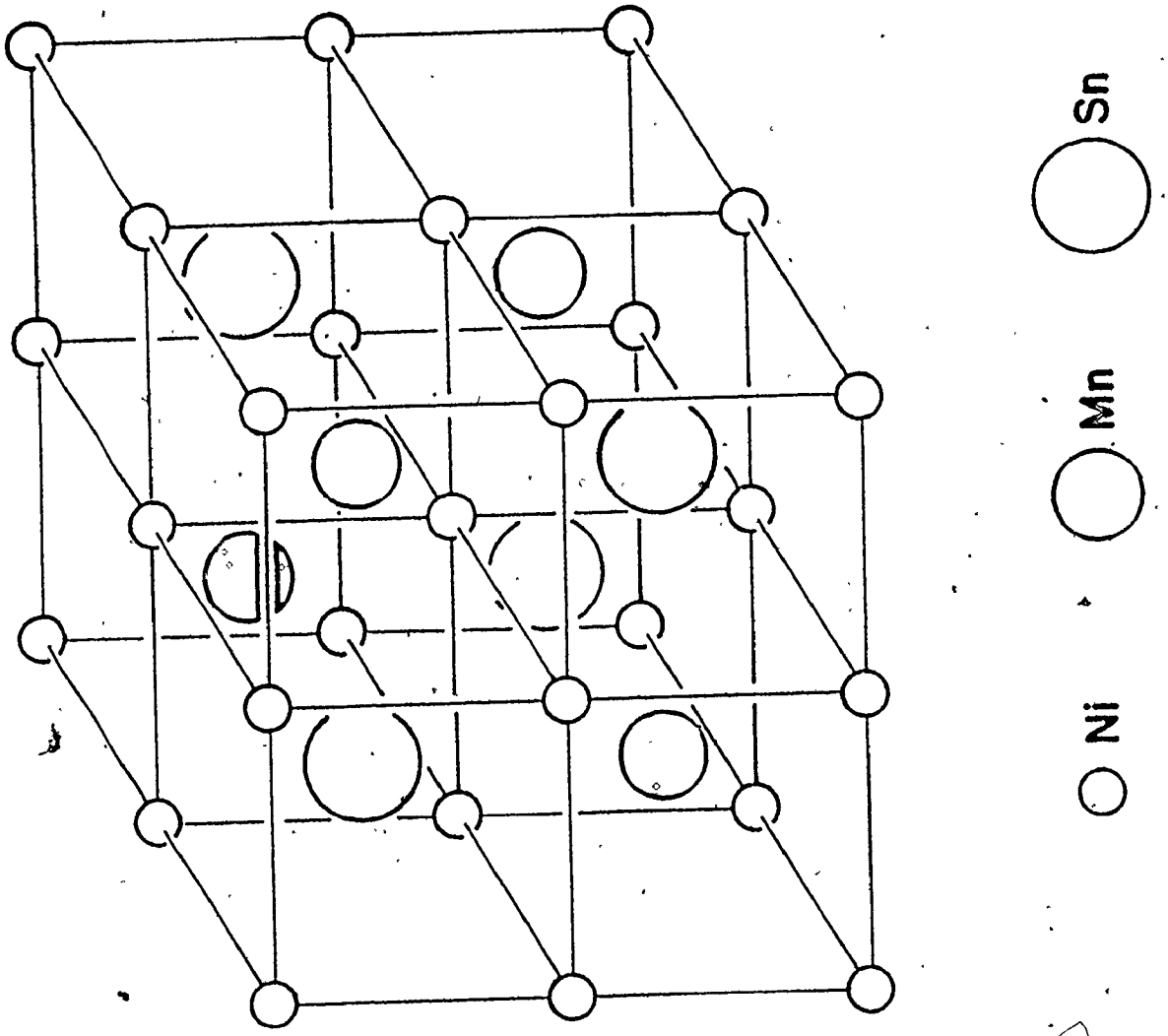
Sn
Mn
Ni

interaction in inelastic neutron scattering experiments. Of the many mechanisms proposed for the coupling of these moments only two fit these experiments reasonably well: the interactions proposed by Price (1978) and the ones suggested by Stearns (1979). Price advanced a double resonance exchange model depending on the average conduction electron concentration. Stearns' model involves two types of d-electrons, itinerant d-electrons and localized d-electrons. The d_{it}-d_{loc} exchange contribution, expected by Stearns to dominate the ferromagnetic case, is thought to depend sensitively on the X atom. Webster (1981) carried out an experimental test and found that Price's model is in better agreement with his results.

Campbell (1975) has reviewed measurements of the magnetic hyperfine fields acting on the non-Mn nuclei in a large number of Heusler alloys. The magnitude and sign of these fields give information on the spin polarization of the conduction electrons which are responsible for the indirect magnetic interaction between the Mn atoms. There have been extensive magnetization and crystallographic measurements made on Heusler alloys. The review by Campbell (1975) gives extensive references to lattice parameter and magnetization determinations. Of particular interest is the work by Campbell and Stager (1976) on the system $Ni_2Mn_xV_{1-x}Sn$.

Since the beginning of the work on Heusler alloys it has been known that chemical order plays an important role in the magnetic properties. Few experimenters studied it systematically due probably to the difficulties in controlling it. Webster (1967, 1969) studied the effect of heat treatment on polycrystalline Pd_2MnIn, Pd_2MnSn and

Pd_2MnSb. The first one of these showed an obvious increase in disorder if it was quenched rather than slow-cooled from 800°C. There is also a marked alteration of the magnetic properties. For the two other systems, he concluded that they were unaffected by heat treatment. His results for chemical order are reproduced in Table I-1.

Table I-1: Atom by crystal site.

		A or C	B	D
Pd_2MnIn (slow-cooled)				
	Pd	.96	.04	.04
	Mn	.02	.89	.07
	In	.02	.07	.89
Pd_2MnIn (quenched)				
	Pd	.96	.04	.04
	Mn	.02	.67	.29
	In	.02	.29	.67
Pd_2MnSn				
	Pd	.99	.01	.01
	Mn	.005	.985	.005
	Sn	.005	.005	.985
Pd_2MnSb				
	Pd	.80	.00	.40
	Mn	.00	1.00	.00
	Sb	.20	.00	.60

These results were derived from quantitative measurements of the three first neutron diffraction peaks of powder specimens. The measurements were taken at two different temperatures to allow an average Debye-Waller factor to be evaluated. He assumed a mean atomic weight and fitted a single Debye temperature. Qualitative x-ray measurements were also performed. Distinguishing between Pd, Sn and Sb is difficult with x-rays as the atomic numbers are very close: 46, 50 and 51. The neutron scattering lengths are very similar: 6.0, 6.1 and 5.6 fm. In view of the errors in the scattering lengths, Webster's precision seems remarkable. He quotes no errors or precision.

Using Mössbauer spectroscopy, Birchall et al (1980 a,b) studied the series $Ni_2Mn_xV_{1-x}Sn$ and $Pd_2Mn_xV_{1-x}Sn$. Their results on powder specimens suggested that significant amounts of disorder occurred: v.g. 22% Ni$\longleftrightarrow$Sn disorder in Ni_2MnSn, 37% Pd$\longleftrightarrow$Sn in $Pd_2Mn_{.6}V_{.4}Sn$. As well, Sobczak (1979) explains the differences between his magnetization results and those of Campbell and Stager (1976) by postulating chemical disorder, e.g. 10% Mn$\longleftrightarrow$Sn disorder in his polycrystalline Ni_2MnSn sample.

These large Mn$\longleftrightarrow$Sn disorders were of great concern in a concurrant investigation of the spin-waves in $Ni_2Mn_{.8}V_{.2}Sn$ (Locke et al, 1981). One of the major purposes of this thesis is to carefully investigate the chemical disorder in single crystal samples of $Ni_2Mn_xV_{1-x}Sn$. A preliminary investigation of chemical disorder in a single crystal of $Ni_2Mn_{.8}V_{.2}Sn$ has been previously carried out in this laboratory (Locke, Master's thesis, 1977, unpublished).

CHAPTER II

THEORY

In this chapter the theory of diffraction of neutrons by crystals will be reviewed. The material given here is only intended as an outline, more details may be found in one of the many monographs on the subject (e.g. Marshall and Lovesey, 1971, and Bacon, 1975).

This chapter divides into the following sections: Scattering Theory, Nuclear Scattering, Debye-Waller Factor, Thermal Diffuse Scattering, Magnetic Scattering, Rotating Crystal Method, Absorption, Extinction and Structure Factor Calculation.

A. Scattering Theory

Suppose that a crystal is set right in the path of a thermal neutron beam. Different types of measurements could be made on such a system. The obvious ones are all related to how the neutrons are deflected by the crystal. These measurements in each case can be expressed in terms of quantities known as "cross-sections". The interesting task is to make the connection between the properties pertaining to the crystal and the cross-sections. Because of the nature of the problem, neutrons of thermal energy colliding with a crystal built up of atoms, the solution to this problem is undertaken in the general frame of Quantum Mechanics.

The problem of calculating the neutron scattering cross-sections is set up as follows. A polar co-ordinate system is arranged so that a beam of incoming neutrons is travelling in the positive z-direction. It impinges on a scatterer at the origin which deflects the neutrons through the polar angle θ in some direction defined by the azimuthal angle ϕ. The incident and scattered neutrons are described as plane waves with propagation vectors $\vec{k}$ and $\vec{k}'$ respectively. The flux of incident neutrons, Φ, is defined as the number of particles incident on the scatterer per unit area per unit time.

The cross-section for a scattering arrangement of N atoms is

$$\sigma = (\text{number of scattered particles per unit time})/\Phi N d\Omega$$

The differential cross-section is defined as

$$\frac{d\sigma}{d\Omega} = (\text{number of scattered particles per unit time into the solid angle } d\Omega \text{ in the direction } \theta, \phi)/\Phi N d\Omega$$

Similarly, the partial differential cross-section is defined such that

$$\frac{d^2\sigma}{d\Omega\, dE'} = (\text{number of scattered particles per unit time into the solid angle } d\Omega \text{ in the direction } \theta, \phi \text{ with final energy between } E' \text{ and } E' + dE')/\Phi N d\Omega\, dE'.$$

The relationship between the various cross-sections is obvious and can be expressed as

$$\sigma = \int_{\substack{\text{all}\\\text{direction}}} \frac{d\sigma}{d\Omega}\, d\Omega = \int_0^\infty \int_{\substack{\text{all}\\\text{direction}}} \frac{d^2\sigma}{d\Omega dE'}\, d\Omega dE'$$

Let the initial state of the system be described by the ket $|\vec{k}sn\rangle$ where $\vec{k}$ refers to the neutron wave vector, s the neutron spin, and n the initial state of the scatterer. Similarly, let $|\vec{k}'s'n'\rangle$ represents the state of the neutron and scatterer after scattering. It is readily seen that the partial differential cross-section is a measure of the probability of transition from the state defined by the ket $|\vec{k}sn\rangle$ to the one defined by $|\vec{k}'s'n'\rangle$. This probability can be derived from Fermi's "Golden rule" to give

$$\frac{d^2\sigma}{d\Omega dE'} = \frac{k'}{k}\left(\frac{m}{2\pi\hbar^2}\right)^2 \sum_{ns} p_n p_s \sum_{n's'} |\langle \vec{k}'s'n'|\hat{V}|\vec{k}sn\rangle|^2 \delta(\hbar\omega + E_n - E_n') \quad \text{(II-1)}$$

where $\hat{V}$ is the interaction potential that causes the transition, $p_s p_n$ are the probabilities that the incoming neutron has spin s and that the scatterer is in the state described by n. The probabilities can be calculated by use of statistical mechanics. The summation over all the

final states (s', n'), that have wave vector $\vec{k}'$, and averaging over all initial states (s,n), with wave vector $\vec{k}$, is necessary in order to obtain the total partial differential cross-section for all possible scattering processus. The delta-function builds into the equation the conservation of energy condition

$$\frac{\hbar^2 k^2}{2m} + E_n = \frac{\hbar^2 k'^2}{2m} + E_n'$$

where

$$\frac{\hbar^2}{2m}(k^2 - k'^2) = \hbar\omega$$

E_n and E_n' are the initial and final energies of the scatterer.

B. Nuclear Scattering (from bound nuclei)

When a neutron is scattered by a nucleus, the nucleon-nucleon interaction is responsible. This is known to have a very short range, approximately 1.5×10^{-5} Å, much less than the wavelength of a thermal neutron, which is typically of the order of 1 Å. Thus the scattering is isotropic, containing only s-wave components. It is well known that this type of scattering can be characterized by a single complex parameter b, called the scattering length. The imaginary part describes absorption processes such as radiative capture. In general, the scattering length is different for each element and isotope and is also sensitive to the relative spin orientations of the scatterer and the neutron.

The only form of $\hat{V}(\vec{r})$ that, using the Born approximation, gives isotropic scattering is a delta-function. If the nucleus is at a position defined by $\vec{R}$, the Fermi pseudo-potential is defined as

$$\hat{V}(\vec{r}) = \frac{2\pi\hbar^2}{m} b\delta(\vec{r} - \vec{R})$$

This Fermi pseudo-potential is a formal artifice defined to give, in the Born approximation, what is known to be correct for simple s-wave scattering. It is not the true potential. Nevertheless it will be the one used in the following derivation with for only justification the fact that it gives the right s-wave scattering.

If this picture is extended to a crystal,

$$\hat{V}(\vec{r}) = \frac{2\pi\hbar^2}{m} \sum_{\vec{l}} \sum_{\vec{d}} b_{\vec{l}\vec{d}} \delta(\vec{r} - \vec{l} - \vec{d}) \qquad \text{(II-2)}$$

where $\vec{l}$ is a lattice vector from the origin to the origin of the unit cell at $\vec{l}$, $\vec{d}$ is a vector from the origin of the unit cell to the atom at $\vec{d}$ in the unit cell. Substituting equation (2) in equation (1) and assuming that the energy of the crystal is independent of the isotope distribution and the nuclear spin orientations, allows one to derive the following expression for the elastic differential cross-section.

$$\left(\frac{d\sigma}{d\Omega}\right)^{elast} = \left(\frac{d\sigma}{d\Omega}\right)^{elast}_{coh} + \left(\frac{d\sigma}{d\Omega}\right)^{elast}_{incoh}$$

where

$$\left(\frac{d\sigma}{d\Omega}\right)^{elast}_{coh} = N\frac{(2\pi)^3}{v}\sum_{\vec{G}}\delta(\vec{K} - \vec{G})\,|F_N(\vec{G})|^2 \qquad \text{(II-3)}$$

$$\left(\frac{d\sigma}{d\Omega}\right)^{elast}_{incoh} = N\sum_{\vec{d}}\left(\overline{|b_{\vec{d}}|^2} - |\overline{b_{\vec{d}}}|^2\right)$$

$$F_N(\vec{G}) = \sum_{\vec{d}}\overline{b_{\vec{d}}}\exp(i\vec{G}.\vec{d}) \qquad \text{(II-4)}$$

$F_N(\vec{G})$ is called the structure factor, N is the number of unit cells in the crystal, v is the volume of a unit cell, $\vec{K} = \vec{k} - \vec{k}'$, the scattering vector and $\vec{G}$ is a reciprocal lattice vector. The $\overline{b}$'s are determined experimentally and are tabulated for pure elements (v.g. Bacon, 1975). The bar over b denotes an averaging over anything that

occupy that position in the unit cell. It is an average over spin orientations, if any, and also over different isotopes. If there are more than one element on that particular site of the crystal this averaging includes the different chemical species.

The two parts of the differential cross-sections are profoundly different. The coherent one can be very large if some geometrical conditions are satisfied, or it can vanish. The incoherent scattering is isotropic. From now on the discussion will be restricted to the coherent scattering.

At this particular step of the discussion it is interesting to point out that the delta-function built into the differential cross-section is the well known Bragg's law, but in a different formulation. To see this, one writes

$$\delta(\vec{K} - \vec{G}) \rightarrow \vec{K} = \vec{G}$$

with

$$\vec{K} = (\vec{k} - \vec{k}')$$

and

$$\vec{G} = \frac{2\pi}{d_{hkl}}$$

d_{hhl} is the distance between the successive planes of Miller indices h, k and l. If the angle between $\vec{k}$ and $\vec{k}'$ is called 2θ, as $|\vec{k}| = |\vec{k}'|$ then

$$|\vec{G}| = |\vec{k} - \vec{k}'|$$

$$|\vec{G}| = 2k \sin\theta$$

with

$$k = \frac{2\pi}{\lambda}$$

therefore

$$|\vec{G}| = \frac{2\pi}{d_{hkl}}$$

$$|\vec{G}| = \frac{4\pi \sin\theta}{\lambda}$$

and finally

$$\lambda = 2d_{hkl}\sin\theta$$

C. Thermal Motion and Debye-Waller Factor

The rigid lattice model does not fit reality perfectly. The atoms that make up a crystal undergo vibrations due to thermal excitation. If these vibrations are assumed to be harmonic oscillations about their mean positions, the structure factor becomes

$$F_N(\vec{G}) = \sum_{\vec{d}} \bar{b}_{\vec{d}} \exp(i\vec{G}.\vec{d}) \exp(-W_{\vec{d}}(\vec{G})) \qquad \text{(II-5)}$$

where

$$W_{\vec{d}}(\vec{G}) = \tfrac{1}{2}\langle(\vec{G}.\vec{U}_{\vec{d}})^2\rangle$$

In cubic crystals,

$$W_{\vec{d}}(\vec{G}) = \frac{1}{6}\vec{G}^2\langle U_{\vec{d}}^2\rangle \qquad \text{(II-6)}$$

The $W_d(\vec{G})$'s are called Debye-Waller factors. For cubic crystals they are proportional to the mean squared displacement $\langle U_d^2 \rangle$. The Debye-Waller factors cause a reduction in the intensities that increases with $G \propto \sin\theta/\lambda$ and temperature. Because the Debye-Waller factors are different for each atomic species, they do not enter $F_n(\vec{G})$ as a simple exponential scaling factor.

D. Thermal Diffuse Scattering

The following discussion of thermal diffuse scattering closely follows that given by Cooper (1970).

Thermal motion of atoms not only reduces the elastic cross-section via the unit cell structure factor, but also gives rise to inelastic scattering processes (creation or annihilation of one or more phonons). All detectors have a finite energy resolution. Therefore they detect some of these inelastically scattered neutrons called thermal diffuse scattering (TDS). It is expected that for multi-phonons scattering the effect is to produce a uniform background easily discarded by a standard background correction. The one phonon scattering is more troublesome, peaking under the Bragg peak. For neutrons that travel much faster than the velocity of sound in the crystal, the correction is the well known one of x-rays. For neutrons that travel slower than the velocity of sound in the crystal, the scattering is expected to be uniform, and the correction is easily applied. Cooper (1970) has also considered the case when the neutron velocity is just slightly larger than the sound velocity. He showed

that, to a good approximation for cubic crystals, neglecting the thermal diffuse scattering causes an apparent reduction in the Debye-Waller factor, the other parameters being unaffected.

Although the velocity of sound in Heusler alloys is not known, the velocity of sound in 3 of the transition metals, which should be comparable, are larger than or of the order of the velocity of the neutrons used in this work, (v (λ = 1.47 Å) = 2.65 Km/s.). As a result, no TDS corrections other than simple background substraction were applied. As a consequence, the Debye-Waller factors may not be reliable.

E. Magnetic Scattering

A neutron, although a neutral particle, has a magnetic moment. Hence neutrons can interact with any magnetic structure and give additional interference effects. In a crystal, the interaction is provided by the unpaired electrons. The effect of that interaction is different for a paramagnet than for an ordered magnetic material. For a paramagnet in zero magnetic field, there is no coherent magnetic scattering. For a ferromagnet studied with unpolarized neutrons, the elastic coherent differential cross-section splits into two parts

$$\left(\frac{d\sigma}{d\Omega}\right)_{\text{coh}}^{\text{elast}} = \left(\frac{d\sigma}{d\Omega}\right)_{\text{nuclear coh}}^{\text{elast}} + \left(\frac{d\sigma}{d\Omega}\right)_{\text{magnetic coh}}^{\text{elast}}$$

No interference effects appear between these two terms of different origins. For cubic crystal, the magnetic elastic coherent differential cross-section is

$$\left(\frac{d\sigma}{d\Omega}\right)^{\text{elast}}_{\substack{\text{mag}\\ \text{coh}}} = \frac{2}{3}N\frac{(2\pi)^3}{v}\sum_{\vec{G}}\delta(\vec{K}-\vec{G})\left|F_M(\vec{G})\right|^2 \qquad \text{(II-7)}$$

where

$$F_M(\vec{G}) = \sum_{\vec{d}} P_{\vec{d}}\frac{g_{\vec{d}}}{2}\exp(i\vec{G}.\vec{d})\exp(W_{\vec{d}}(\vec{G})) \qquad \text{(II-8)}$$

$$P_{\vec{d}} = \frac{re^2}{m_e c^2}\langle \hat{S}_{\vec{d}}\rangle\left|f_{\vec{d}}(\vec{G})\right| \qquad \text{(II-9)}$$

r is the magnetic moment of a neutron, $g_{\vec{d}}$ is the Landé splitting factor, $\langle \hat{S}_{\vec{d}}\rangle$ is the thermal average of the spin, and $f(\vec{G})$ is known as the form factor. It arises from the spatial distribution of the unpaired electrons. The D.W. factors reduce the coherent magnetic scattering in the same way as they reduce the coherent nuclear scattering.

For $T<\hat{T}c$, the Curie temperature, magnetic scattering, proportional to $\langle \hat{S}\rangle^2$, will be added to the nuclear scattering. As the symmetry of the crystal is not changed by the magnetic ordering, no new Bragg peaks will appear.

F. The Rotating Crystal Method

In a measurement of a Bragg peak the scattered intensity is integrated as the condition

$$\vec{K} = \vec{G}$$

is passed through by varying some experimental parameter. If the differential cross-section, eq. 3, is integrated in a similar manner the delta function is removed and a direct comparison is possible.

The rotating crystal rotates $\vec{G}$. Only when $\vec{G} = \vec{K}$ is scattering observed. This condition, combined with the counter set at the Bragg angle, means that the experimental rotation performs the necessary integrations, so that it is the total cross-section that is measured. A similar manipulation, on equation 3, results, for the integrated intensity, in an expression proportional to a well known crystallographic quantity, i.e.

$$Q_{2\theta} = \frac{\lambda^3 |F_N(\vec{G})|^2}{v^2 \sin 2\theta} \qquad (cm^{-1})$$

where $\frac{1}{\sin 2\theta}$ is the Lorentz factor.

G. Absorption

Neutrons travelling in the crystal are absorbed. As a consequence the flux decreases, and so the measured intensities. This reduction in the intentities is proportional to

$$A = \frac{1}{V} \int_{\text{crystal}} \exp(-M(p + q))\, dV$$

where V is the volume of the crystal, p and q are the lengths of the incident and diffracted paths, M is the linear absorption coefficient.

For simple geometries such as a sphere or a cylinder, analytic expressions for "A" are known. A table of "A" is given by Rouse et al. (1970) for small values of MR, where R is the radius of the sample. This correction is negligible for the samples herein under study.

H. Extinction

Another phenomenon that alters the integrated intensities is extinction. Neutrons travelling through the crystal are Bragg scattered out of the incident beam, depleting the beam, therefore the integrated intensities. Following the argument of Zachariesen (1967) for x-rays, a correction can be calculated.

If $F_o(\vec{G})$ is the observed structure factor, $F(\vec{G})$ the structure factor that would be observed if no extinction were present, then a function $y(\vec{G})$ can be defined so that

$$F_0^2(\vec{G}) = y(\vec{G})F^2(\vec{G}) \qquad \text{(II-10)}$$

where

$$y(\vec{G}) = (1 + 2c\bar{T}Q_{2\theta}(\vec{G}))^{-\frac{1}{2}} \qquad \text{(II-11)}$$

$$Q_{2\theta}(\vec{G}) = \frac{\lambda^3 F^2(\vec{G})}{\sin 2\theta} \qquad \text{(II-12)}$$

$\bar{T}$ is the mean path length in the crystal, c is a constant related to the size and angular spread of the mosaic blocks of the crystal. Cooper et al. (1968) and Cooper and Rouse (1970) have shown for neutrons that this correction is good up to 40% extinction. They also give more complicated expressions to go beyond 40% extinction.

A convenient way to make the correction has been suggested by Bacon & Jude (1973). If we define the ratio $F_o^2(\vec{G})/F^2_{calc}(\vec{G})$ as $y^*(\vec{G})$, where $F_{calc}(\vec{G})$ is the computed value of $F(\vec{G})$ using the experimental reflections, $y^*(\vec{G})$ will be a close approximation of $y(\vec{G})$, since $F_{calc}(\vec{G})$ will be very close to $F(\vec{G})$. This procedure was followed in this work, treating c as an adjustable parameter.

Examination of eq. 11 shows how extinction can be reduced experimentally, that is to say, how to get $y(\vec{G})$ as close to one as possible. Experimentally it is difficult to vary the mosaic block size or angular spread. The mean path length can be reduced by having a thinner crystal, but intensities considerations set a lower limit to this size. Neutrons are available only in relatively low flux. $Q(\vec{G})$ can be drastically diminished by reducing the wavelength, being proportional to λ^3. But $Q(\vec{G})$ is also proportional to the integrated intensities Again a trade off has to be made. Because of the Lorentz factor, $\frac{1}{\mathrm{Sin}2\theta}$ in the equation for $Q(\vec{G})$ it is clear that extinction will be more severe at low or high angles.

I. Structure Factor of $Ni_2Mn_xV_{1-x}Sn$

Ni_2MnSn and Ni_2VSn are isomorphous Heusler alloys of stoichiometric composition X_2YZ. They have the $L2_1$ crystal structure. The allowed reflections and relative intensities are determined by calculating their structure factors. Structure factors are calculated by using eq. (4)

$$F_N(\vec{G}) = \sum_{\vec{d}} \bar{b}_{\vec{d}} \exp(i\vec{G}.\vec{d})$$

$$F_N(\vec{G}) = \sum_{\vec{d}} \bar{b}_{\vec{d}} \exp(2\pi i(\frac{hx_d}{a} + \frac{ky_d}{a} + \frac{lz_d}{a})) \qquad \text{(II-13)}$$

where h, k, l are the Miller indices of the reflection planes corresponding to the reciprocal lattice vector $\vec{G}$, and $\frac{x_d}{a}$, $\frac{y_d}{a}$, and $\frac{z_d}{a}$ are the co-ordinates of the atom at $\vec{d}$ in the unit cell. The Debye-Waller factors have been omitted here. For Ni_2MnSn and Ni_2VSn, there are three groups of allowed hkl reflections. These are described below.

h,k,l all odd eg.(111)

h,k,l all even and h+k+l = 4n+2 eg. (200)

h,k,l all even and h+k+l = 4n eg. (220)

The corresponding structure factors are

$$F_N(111) = 4|b_y - b_z|$$

$$F_N(200) = 4|b_y + b_z - 2b_x|$$

$$F_N(220) = 4|b_y + b_z + 2b_x|$$

(II-14)

For $Ni_2Mn_xV_{1-x}n$, the Y site can be occupied by either a Mn or a V atom since Ni_2MnSn and Ni_2VSn are isomorphous. Furthermore, disorder can occur between X, Y and Z sites, strongly affecting the observed intensities. To obtain agreement between measured and calculated structure factors, one must propose a reasonable model of the disorder. The various disorder parameters can be adjusted to fit predicted to measure intensities. The formulae below and calculations assume that there is no chemical disorder and that all moments are located on the Mn sites.

The nuclear structure factors are given by:

$$F_N(111) = 4|xb_{Mn} + (1 - x)b_V - b_{Sn}|$$

$$F_N(200) = 4|xb_{Mn} + (1 - x)b_V + b_{Sn} - 2b_{Ni}|$$

$$F_N(220) = 4|xb_{Mn} + (1 - x)b_V + b_{Sn} + 2b_{Ni}|$$

(II-15)

The scattering lengths used are given in Table A.1 in appendix

To correct the x=1. sample for magnetic scattering, the magnetic scattering structure factors predicted by this model are calculated. First, the different magnetic scattering lengths for Mn when involved in different reflections have to be determined. The magnetic scattering lengths are given by eq. 9

$$P = \frac{re^2}{m_e c^2} \langle S \rangle f(\vec{G})$$

where $r = -1.913148$. $\langle S \rangle$ has a value of $(1.13 \pm .02)$ at room temperature from the results of Campbell and Stager (1976). The dependance on the reflection planes is through the atomic form factor $f(\vec{G})$. This form factor has been determined experimentally for Mn in Pd_2MnSn by Ishikawa et al. (1976) as a function of

$$\frac{\sin\theta}{\lambda} = \frac{(h^2 + k^2 + l^2)^{\frac{1}{2}}}{2a} = \frac{|\vec{G}|}{4\pi}$$

The atomic form factors in Table A.1 were obtained from their graph. The magnetic structure factors are given by

$$F_M(hkl) = 4 \; |P(hkl)| \qquad \text{(II-16)}$$

CHAPTER III

SAMPLE PREPARATION AND EXPERIMENTAL APPARATUS

A. Crystal Growth

The neutron scattering experiments were performed on three oriented crystals cut from three large single crystal boules. These were grown at McMaster University. Use of the following apparatus was made: An Arthur D. Little "MP" crystal growing facility associated with a 30 KW, 450 KHz Taylor-Winfield RF generator. Power output of the generator was controlled using a pick-up coil and feed back loop circuit. Graphite susceptors, that couple to the RF field and heat up, supported form-fitting alumina crucibles. By this mean a proper mixture of the elements were melted in these crucibles under a purified Ar atmosphere.

Garrett et al. (1979) grew the x=1.0 sample by the Kyropoulos method. In this technique, a seed is lowered over a melt and then the entire melt is cooled. Garrett wetted the seed, expanded it to about 80% of the Coors CH20 crucible diameter and then slow-cooled the entire melt at about 10° K/h.

The Bridgman method was used to grow the x=0.8 and the x=0.6 samples. In this technique a crucible having a conical bottom is utilized. The crucible containing the melt is lowered through a temperature gradient, allowing the tip of the crucible to cool first.

The fine tip, hopefully, allows only one single crystal to grow from the bottom. A temperature gradient of 15° K/cm was used with a melt speed of 1 mm/h.

The large boules were then oriented by means of neutron diffraction. Thin rods with the $[01\bar{1}]$ direction along their axis were cut by spark erosion. The spark cut rods had square cross-sections. The pure and the x=0.8 samples were ground to roughly circular cross-sections. The very small size of the x=0.6 sample and its brittle nature precluded this procedure. The $[01\bar{1}]$ direction coincided with the axis of the samples within 1° for the pure and the x=0.8 sample. The x=0.6 sample had its axis approximately 5° away from the $[0\bar{1}1]$ direction. The sizes of the crystals used are shown in table III-1:

Table III-1: Crystal dimensions

	Ni_2MnSn	$Ni_2Mn_{.8}V_{.2}Sn$	$Ni_2Mn_{.6}V_{.4}Sn$
length	10.2 mm	7.1 mm	18.0 mm
diameter	.74 mm	1.00 mm	.50 x .52 mm

B. The Neutron Spectrometer

All three crystals were studied on the double-axis spectrometer at the McMaster University Reactor (Rowe, 1966). The double-axis spectrometer is extensively documented in the reference. Only the

modes used and changes related to these experiments need to be discussed here.

The basic concept of a thermal neutron spectrometer is to project a collimated beam of monoenergetic neutrons onto a single crystal, or powder specimen, and detect those that scatter off at specific angles. The primary source of thermalized neutrons is a nuclear reactor. In the following discussion, reference is made to the schematic drawing of the McMaster University Reactor spectrometers in Fig. III-1. The neutron beam emerges from a hole in the reactor wall (G). To improve the primary collimation provided by this hole coarse collimators are fitted. The energy distribution of the neutrons is Maxwellian at G. A large single crystal monochromator (X1) samples out a particular wavelength according to Bragg's law

$$\lambda = 2 d_{hkl} \sin \theta$$

where 2θ is the angle made by the reflected beam and the incident beam

d_{hkl} is the d-spacing of the reflecting plane, the atomic interplanar spacing in the [hkl] direction

Two planes of the same monochromator were used in this work. A monochromator rotation mechanism permitted rapid switching between the two planes. The same take-off angle 2θ was used, but the two planes

Fig. III-1: McMaster University Reactor Spectrometers

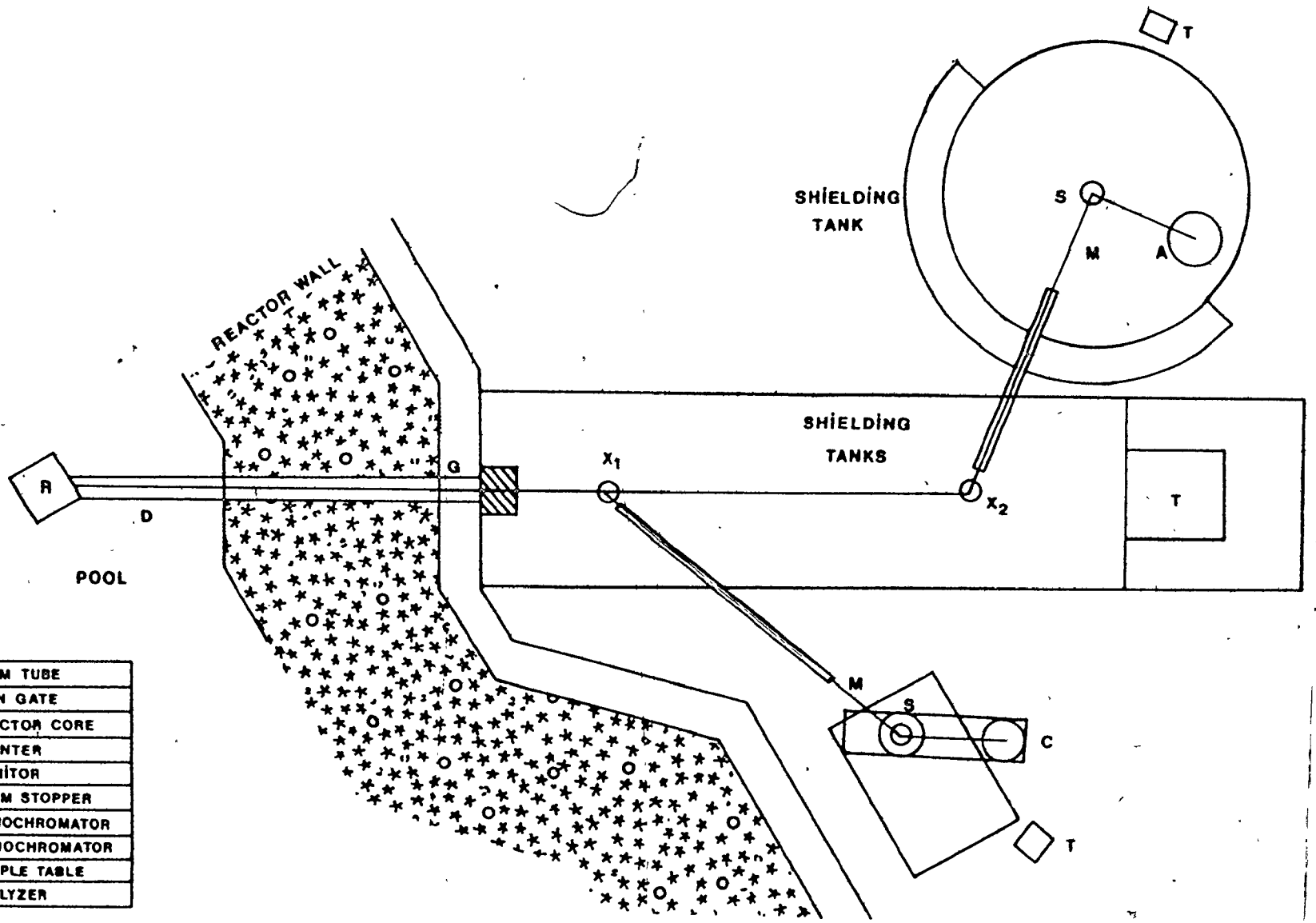

D	BEAM TUBE
G	İRON GATE
R	REACTOR CORE
C	COUNTER
M	MONİTOR
T	BEAM STOPPER
X_1	MONOCHROMATOR
X_2	MONOCHROMATOR
S	SAMPLE TABLE
A	ANALYZER

have different d_{hkl}, atomic interplanar spacing. The monochromator, planes and wavelengths used were:

Aluminum; (200) plane; λ = 1.47 Å

Aluminum; (220) plane; λ = 1.03 Å

The beam, even if it is now essentially monochromatic, has a wavelength spread and an angular divergence due to the monochromator mosaic spread and the angular distribution of the neutrons incident on the monochromator. A large mosaic spread increases the neutron flux at the expense of resolution. High resolution is rarely a necessary condition for single crystal diffraction experiments. The different Bragg peaks are well separated. However, it is particularly important that all of the scattered neutrons are counted so that the integrated intensity can be obtained accurately. A beam gate made of boron in aluminum can be slid into the path of the monochromatic beam. Cadmium irises and slits were used but no Soller slit collimators. The purpose of the irises was to reduce the background counting rate of stray neutrons. The small diameter of the crystals and the large sample-monochromator distance (3.7m) provided sufficient collimation. A fission chamber (M) that intercepts only a small fraction of the beam monitors the incoming flux. The sample table (s) and the counter (c) rotate about common axis.

The specimen table angle is locally referred to as ψ , and the angle that the counter makes with the straight through beam is called ϕ.

The ψ angle is indexed in .05° steps; the ϕ , in .2° steps. The counter is a 5 cm cylinder of high pressure He^3 gas with a detection area of about 32 cm^2, an efficiency of 70% or better and is situated .76 m away from the crystal inside bulky shielding.

The crystals were mounted with epoxy on a thin glass rod, which was glued to a goniometer. The crystals were centered over the table rotation axis by wrapping them in cadmium foil, and taking a picture of them in the beam at different table rotation angle with a Polaroid neutron camera. Cadmium has an enormous neutron capture cross-section, so that the crystal position appeared clearly on the photography. A neutron camera is a scintillating screen made of LiF and ZnS combined with a film holder. Such a picture is shown in Fig. III-2. The white area is a cross-section of the straight through neutron beam. The two dark shadows are cadmium foil resting one at the top of the crystal, one at the foot of it. The crystal itself is not appearing on the picture, being nearly transparent to the beam.

The $[01\bar{1}]$ direction of the crystals was aligned within 20' of a degree with the sample table axis. For this the crystals were set in different reflecting positions, and each time a picture of the diffracted beam was taken. Images of reflections, related by inversion, should coincide if the crystal is perfectly aligned. Fig. III-3 represents this procedure. On the picture appears twice the crystal in the same reflecting position, the camera being smoothly translated between each exposures. The third exposure , the middle one on the picture, represents the crystal rotated by 180°. If

Fig. III-2: Photography of a crystal in the straight through beam.

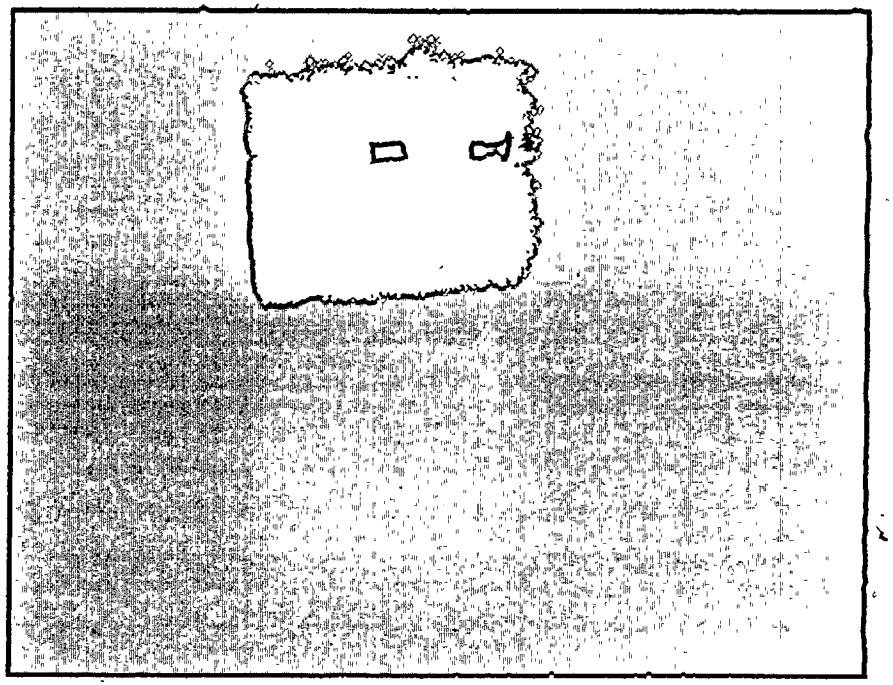

aligned, the three expositions should lie on the same imaginary horizontal line.

ψ was scanned for a number of Bragg peaks while ϕ was set at the 2θ angle for each reflection. The Bragg peaks were scanned in step of .05°. Each time the counter was allowed to record the diffracted neutrons for a preset monitor setting. Great cares were taken to insure that all the scattered neutrons were counted, so that the integrated intensities could be obtained precisely. The scanning range was large enough to get an accurate estimate of the background on each side of the peak. Fig. III-4 gives a typical example of a scan.

Measurements were first done on the $x = 0.8$ sample with $\lambda = 1.47$ Å. Analysis of the data showed that extinction was a sizable effect. The already small size of the crystal made reducing it very difficult. The wavelength was reduced to 1.03 Å and the scans of some peaks were repeated in an attempt to get a measure of the extent of extinction. The same procedure was followed for all the crystals. In addition, for $x = 1.0$ and $x = 0.6$, crystal cross-sections were reduced.

For $\lambda = 1.47$ Å, the $\lambda/2$ contamination is a troublesome quantity. So this was measured by comparing the results of scanning the (022) peak for these two wavelenghts, by setting the detector at their respective 2θ angle for Bragg diffraction. Once corrected for extinction, the ratio λ: $\lambda/2$ was 130:1.

Fig. III-3: Photography of a crystal set in reflecting positions

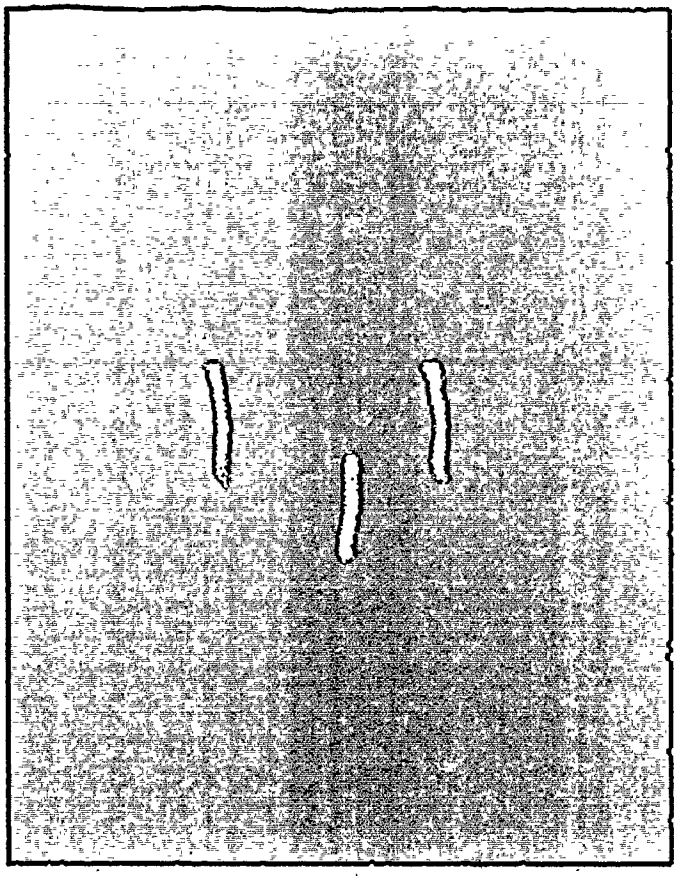

Fig. III-4: Typical Bragg peaks

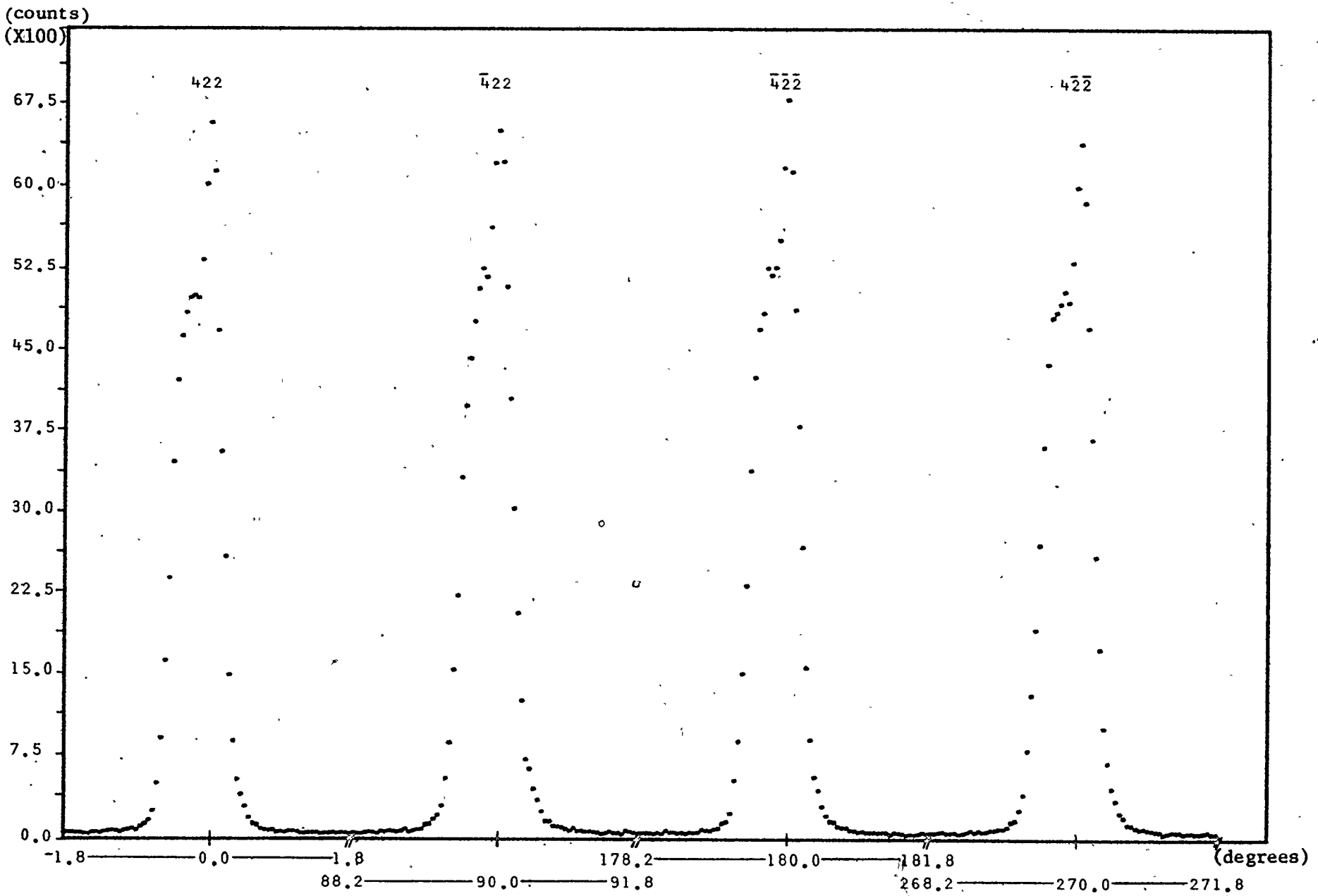
(counts)
(X100)
422
$\bar{4}22$
$\bar{4}\bar{2}\bar{2}$
$4\bar{2}\bar{2}$
67.5
60.0
52.5
45.0
37.5
30.0
22.5
15.0
7.5
0.0
-1.8
0.0
1.8
88.2
90.0
91.8
178.2
180.0
181.8
268.2
270.0
271.8
(degrees)

CHAPTER IV

EXPERIMENTAL DATA AND DISCUSSION

In this chapter the experimental data on $Ni_2Mn_xV_{1-x}Sn$, x=1.0, 0.8 and 0.6, will be presented. The information sought is the chemical ordering.

If one plots the number of counts versus the angle, a histogram is obtained. A typical histogram is shown in Fig. III-4. The area under a Bragg peak can be approximated by summing the counts taken at each step and substracting the background. Care should be taken to insure that the total angle scanned is large enough to give a good measure of the background. Background is predominately the result of incoherent scattering by the sample.

Error occurs because of the statistical nature of counting experiments. The statistical error on a count N_i is $(N_i)^{\frac{1}{2}}$. There is also an error on N_i due to the statistical error in the monitor counting. If M is the monitor setting, this error is $N_i/M^{\frac{1}{2}}$. The sum of these statistical errors on N_i is

$$\Delta N_i = (N_i + N_i^2/M)^{\frac{1}{2}} \qquad \text{(IV-1)}$$

The error on the sum over all the intervals i, $N = \Sigma N_i$, is

$$\Delta N = (N + \Sigma N_i^2 / M)^{\frac{1}{2}} \qquad \text{(IV-2)}$$

The precision on N can be increased at the expense of lengthening the counting time.

The measurements and the calculated statistical errors are shown in tables A-2 in appendix, where for each crystal the Miller reflection indices, the scattering angles, and the counts with their errors are given. The scattering angle is a function of the neutron wavelength. The counts were normalized to 50,000 monitor counts. Different monitor setting were used for different peaks. The monitor settings were chosen so that the statistical error was less than 1%.

Next, the data are averaged over symmetry related reflections, corrected for the Lorentz factor and for $\lambda/2$ contamination. In addition the data for x = 1.0 required correction for coherent magnetic scattering according to table A-1, as explained in Section II-I. These corrected data are presented in table A-3 in appendix along with the reflection indices, $(\sin\theta / \lambda)^2$, and the logarithm of the corrected data. The table is divided into three sections corresponding to the three structure factor groups. The logarithms are plotted versus $(\sin\theta/\lambda)^2$ in Fig. IV-1. The statistical errors on the data are smaller than the size of the points.

For x = 1.0 and x = 0.8, it is obvious that the (022) point falls below the (004) point. This is inconsistent with an exponential

decrease caused only by the Debye-Waller factor. The same effect is observed but to a smaller degree for all the low angle intense reflections, see (200) and (111). As well, the more intense reflections, i.e. the five top points in the group h+k+l = 4n, are a lot more scattered then the ones for the two other structure factor group, i.e. (111) and (200). This is the signature of extinction.

To have a measure of the extent of extinction present in the three samples, the scans of some peaks were repeated at a shorter wavelength. This is one way to reduce extinction, as explained in section II.H. The results are given in tables A-4 and A-5 in appendix. No absolute measurements were done, thus the results were normalized to the point (222) of the previous set. The short wavelenght points are also shown on Fig. IV-1. The distance between the different structure factor groups increases significatively, showing that extinction is a sizeable effect; the less important but persistant scattering of the points for the top group shows that it is still a problem. A correction for extinction is calculated as part of the iterative procedure to calculate the structure factors. Because of the numerous parameters to be calculated in the procedure, the more extensive first set of data is used. Because of the small number of data points available, the extinction is assumed to be isotropic, depending only on the intensity of the reflection. Then the correction discussed in section II-H is used. The correction is added to the formulae II-14, extended for D.W. factor, in table IV-1. The site symmetries for all the atoms are sufficiently high to demand that the Debye-Waller factors be isotropic. Preliminary results showed it

Table IV-1: Formulae used in the fitting

$$b_z = x b_{Mn} + (1-x) b_v$$

II-11 $$y(hkl) = \left[1 + 2c\bar{T}Q^{2\theta}(hkl)\right]^{-\frac{1}{2}}$$

II-12 $$Q^{2\theta}(hkl) = \frac{\lambda^3 \left[F^*(hkl)\right]^2}{\sin 2\theta(hkl)}$$

II-15 $$F^*(111) = k\left[b_{Sn}\, e^{-(B_{Sn}\sin\theta)/\lambda} - b_z\, e^{-(B_z\sin\theta)/\lambda}\right]$$

$$F^*(200) = k\left[2b_{Ni}\, e^{-(B_{Ni}\sin\theta)/\lambda} - b_{Sn}\, e^{-(B_{Sn}\sin\theta)/\lambda} - b_z\, e^{-(B_z\sin\theta)/\lambda}\right]$$

$$F^*(400) = k\left[2b_{Ni}\, e^{-(B_{Ni}\sin\theta)/\lambda} + b_{Sn}\, e^{-(B_{Sn}\sin\theta)/\lambda} + b_z\, e^{-(B_z\sin\theta)/\lambda}\right]$$

IV-3 $$\sigma_{F^*(hkl)} \propto \frac{F^*(hkl)}{Q} \times \left[Q^{2\theta}(hkl)\right]^{\frac{1}{2}}$$

IV-4 $$\chi^2_\nu = \sum_{hkl}\left[\frac{\left\{F_{exp}(hkl) - \sqrt{y(hkl)} \times F^*(hkl)\right\}^2}{\sigma^2_{F^*(hkl)}}\right]$$

IV-5 $$R = \left\{\frac{\sum_{hkl}\left[\frac{1}{\sqrt{y(hkl)}} F_{exp}(hkl) - F^*(hkl)\right]}{\sum_{hkl}\left[\frac{F_{exp}(hkl)}{\sqrt{y(hkl)}}\right]}\right\} \times 100$$

Fig. IV-1: Ln Io vs $(\sin\theta / \lambda)^2$ for nuclear peak intensities Io

a) x=1.0

. λ =1.47 Å
x λ =1.03 Å

(022) (400)

(422)

(044)

(444)

(200) (222)

(244)
(600)

(622)

(111) (311)

(133)

(333)
(511)

(533)

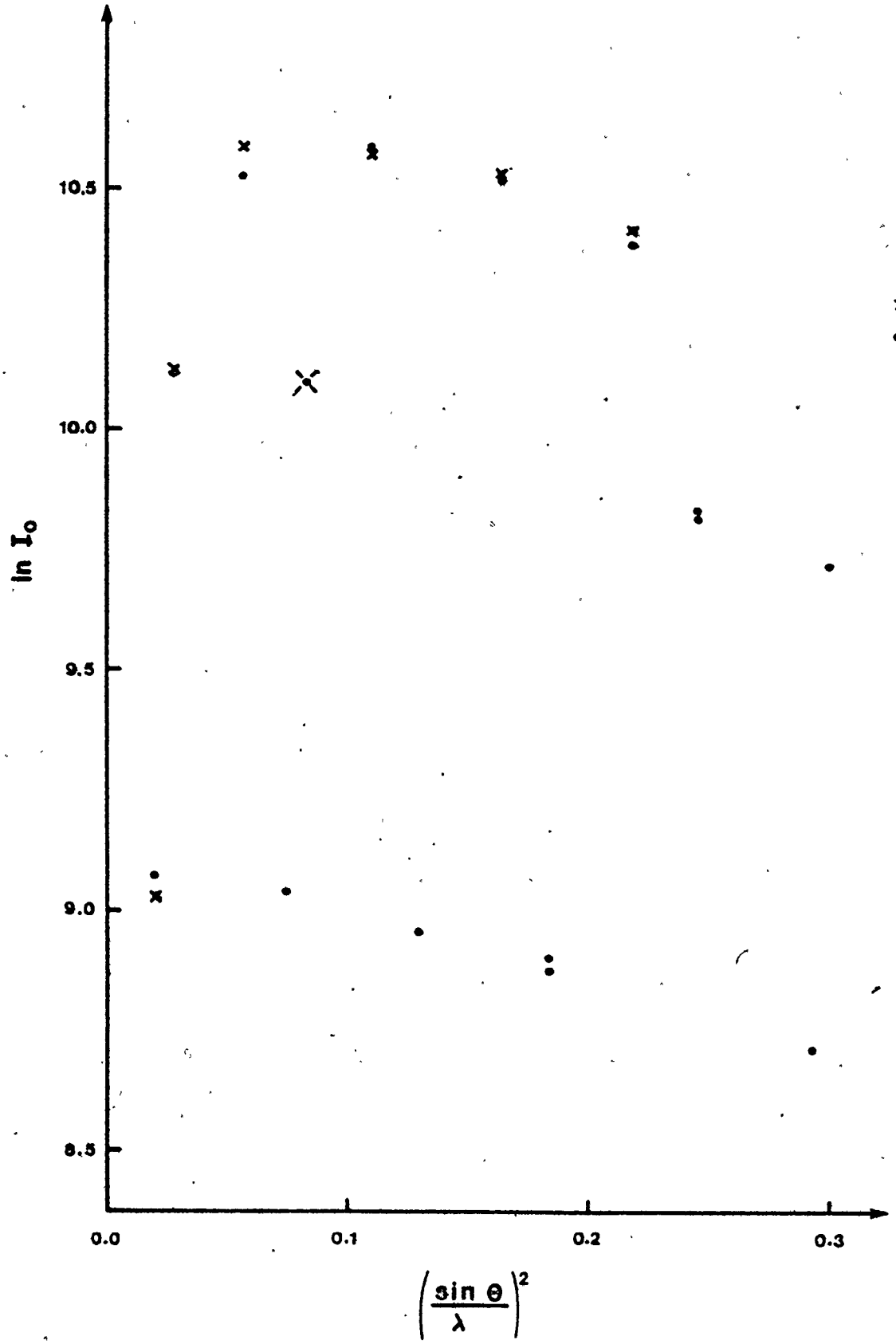
10.5
10.0
9.5
9.0
8.5
ln I_o
0.0
0.1
0.2
0.3
$\left(\frac{\sin\theta}{\lambda}\right)^2$

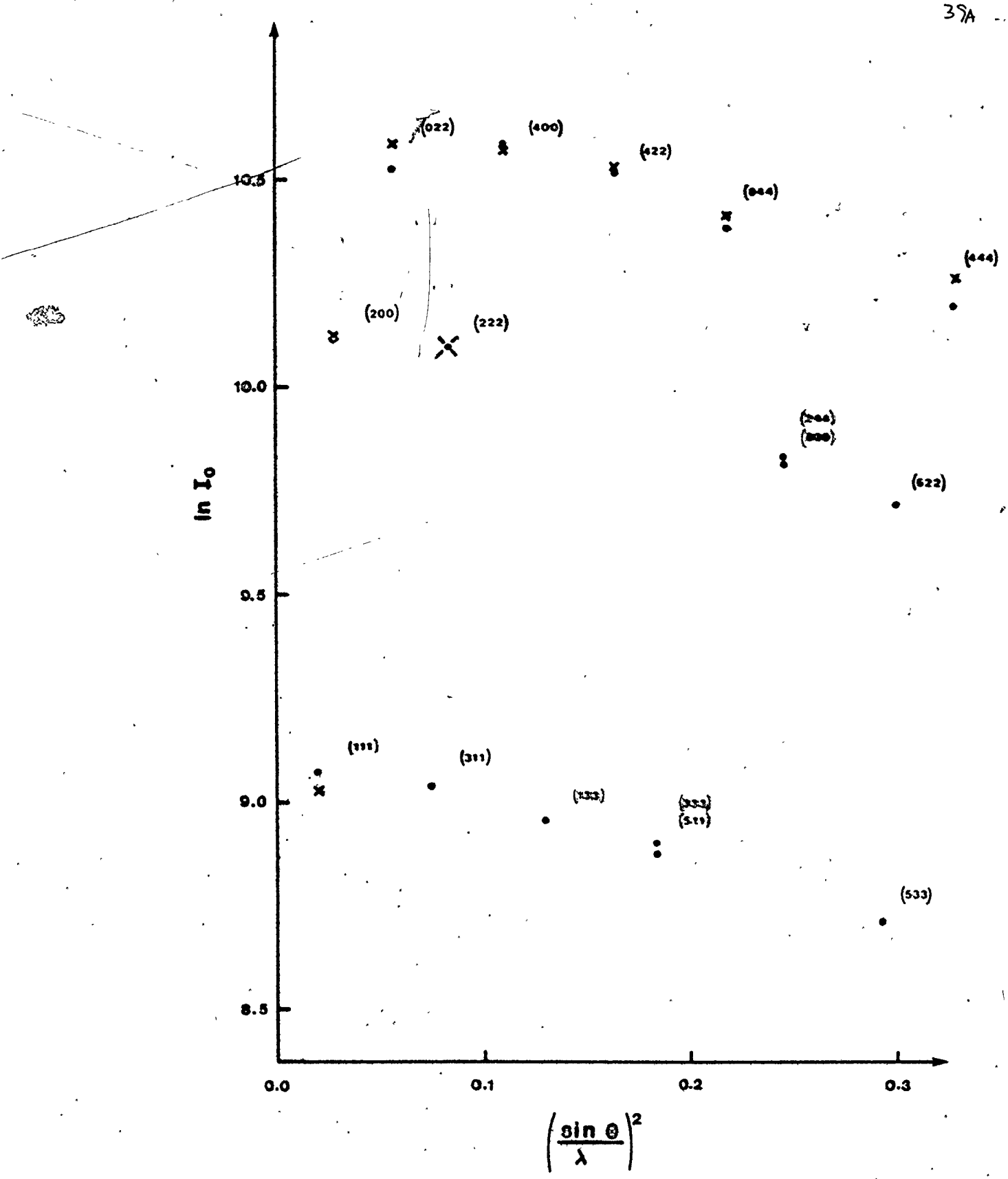
(022)
(400)
(422)
(044)
(444)
(200)
(222)
(244)
(622)
(111)
(311)
(133)
(533)
10.5
10.0
9.5
9.0
8.5
ln I₀
0.0
0.1
0.2
0.3
(sin θ/λ)²

Fig. IV-1: $\ln I_o$ vs $(\sin\theta / \lambda)^2$ for nuclear peak intensities I_o

b) x=0.8

. λ =1.47 Å
x λ =1.03 Å

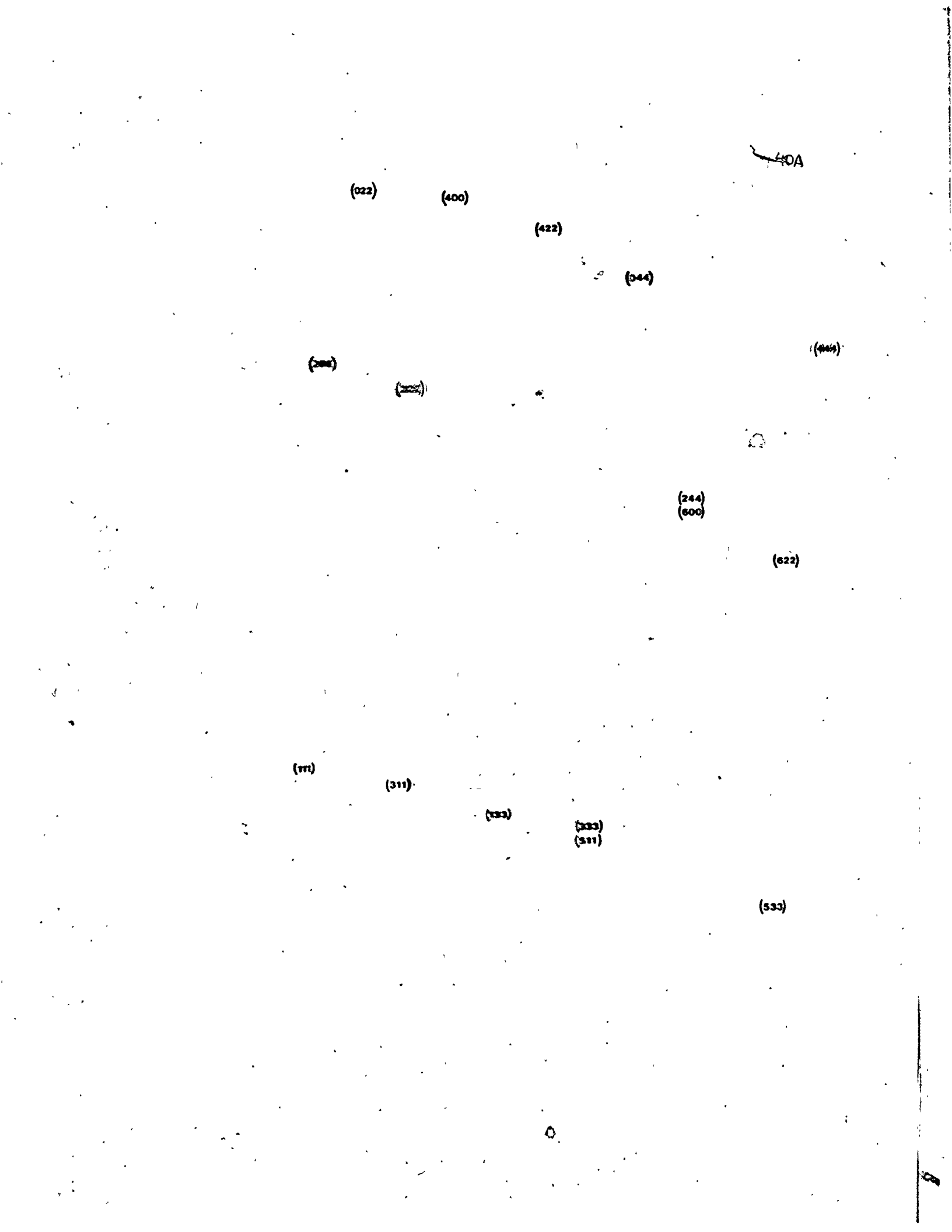
40A
(022)
(400)
(422)
(044)
(244)
(600)
(622)
(111)
(311)
(533)

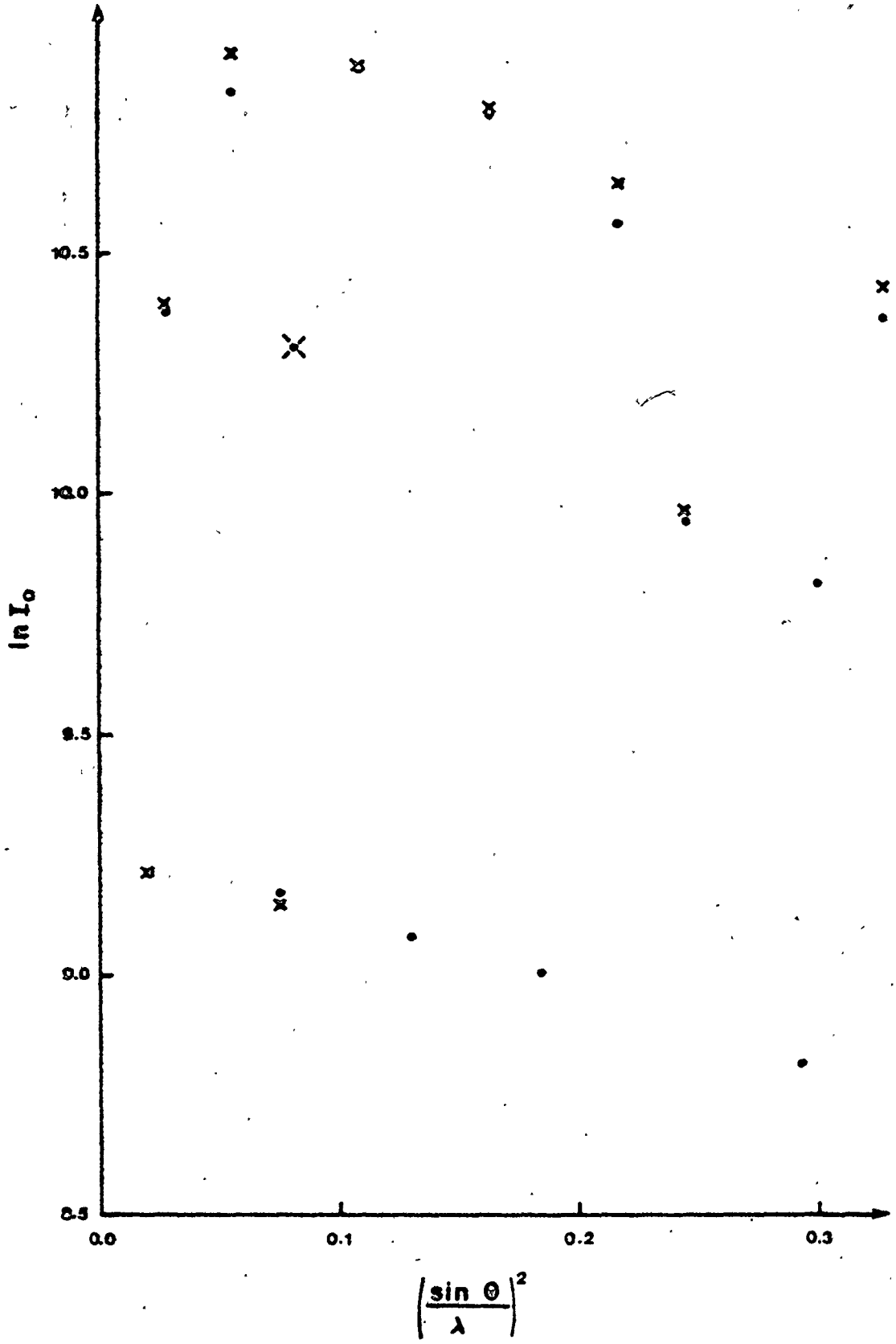
10.5
10.0
9.5
9.0
8.5
ln I_o
0.0
0.1
0.2
0.3
$\left(\frac{\sin \theta}{\lambda}\right)^2$

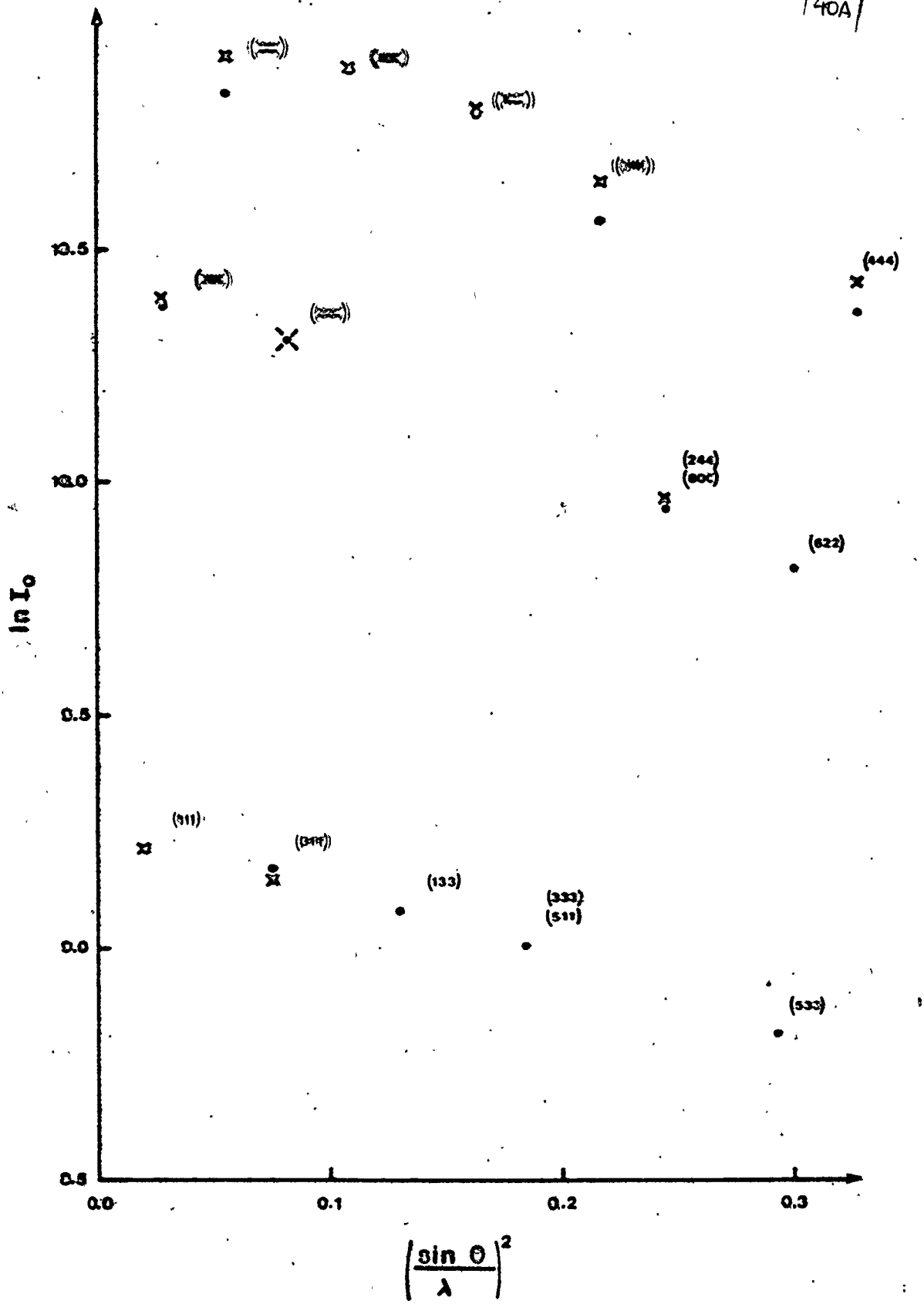
ln I_o
12.5
12.0
0.5
0.0
-0.5
0.0
0.1
0.2
0.3
$\left(\frac{\sin\theta}{\lambda}\right)^2$
(444)
(244)
(800)
(622)
(511)
(133)
(333)
(511)
(533)

Fig. IV-1: ln Io vs $(\sin\theta / \lambda)^2$ for nuclear peak intensities Io

c) x=0.6

• λ =1.47 Å
x λ =1.03 Å

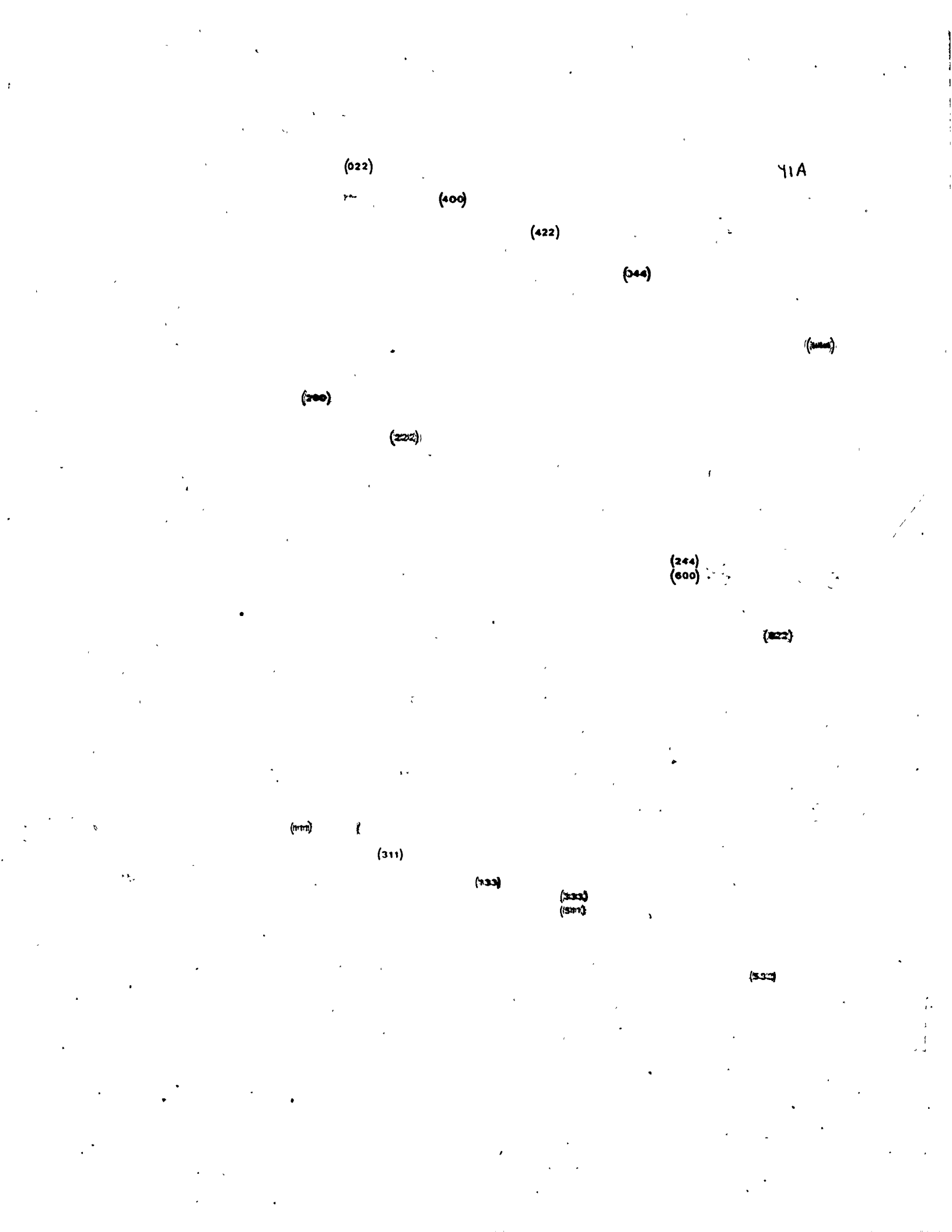
(022)
(400)
(422)
(044)
(200)
(222)
(244)
(600)
(822)
(111)
(311)
(133)
(331)
(511)
(533)

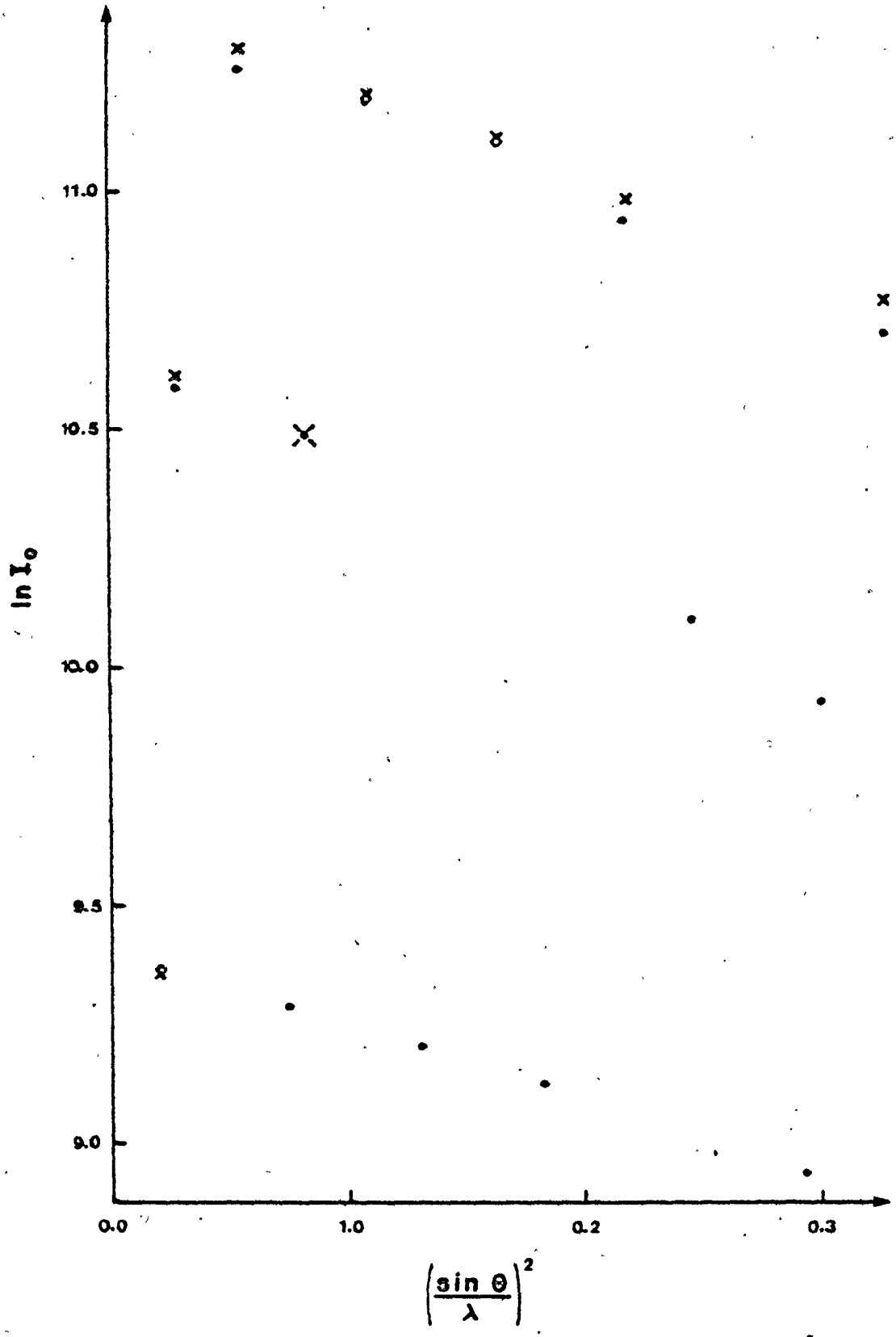
11.0
10.5
10.0
9.5
9.0
ln I₀
0.0
1.0
0.2
0.3
(sin θ / λ)²

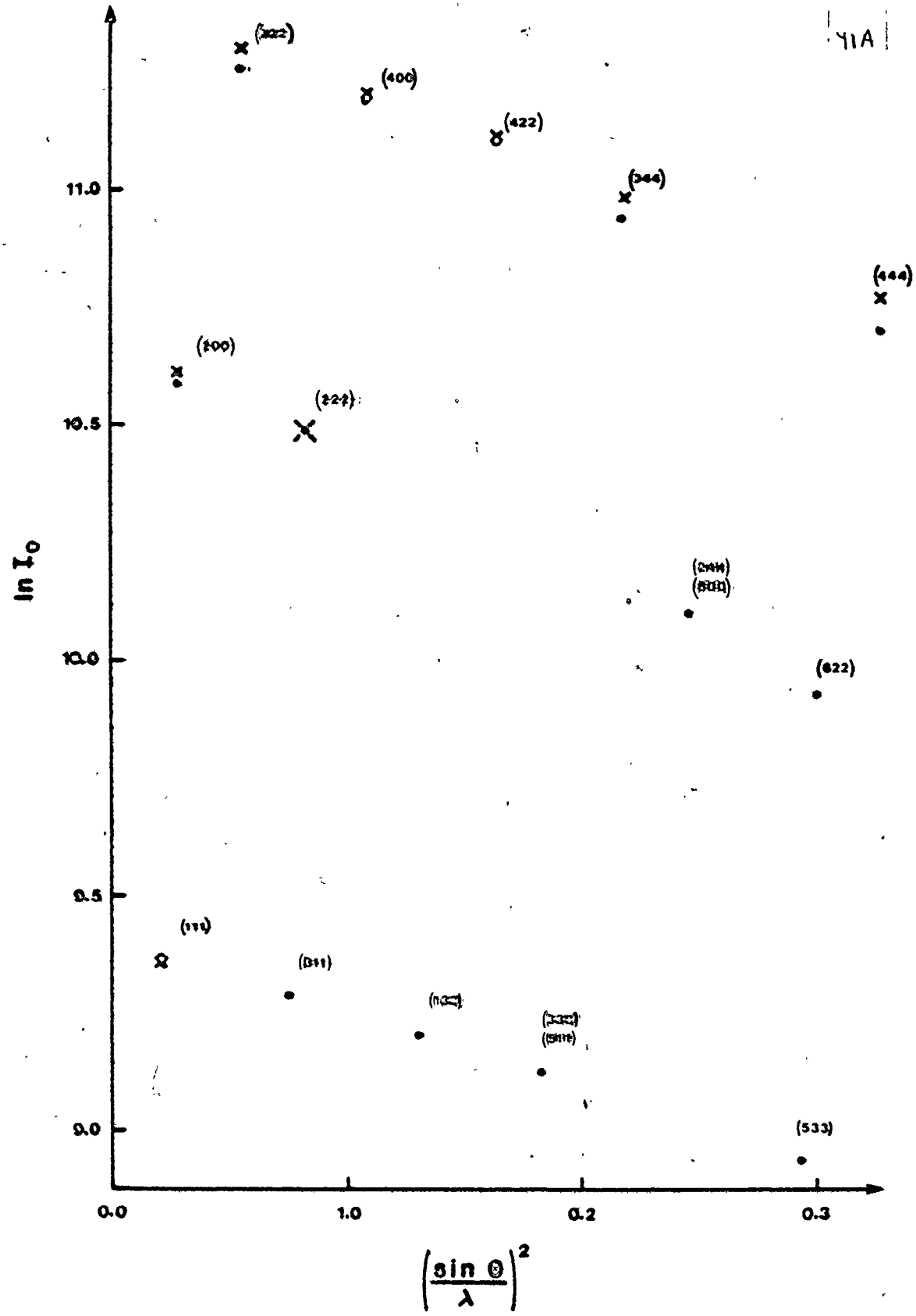
(422)
(400)
(422)
(444)
(444)
(200)
(222)
(622)
(111)
(311)
(533)
11.0
10.5
10.0
9.5
9.0
ln I₀
0.0
1.0
0.2
0.3
(sin θ/λ)²

impossible to distinguish the Debye-Waller factors of Mn and V on the same site. So a single Debye-Waller factor is used for both. As V and Mn have sensibly the same mass, this is reasonable.

The experimental points are fitted to this model, where the quantity fitted is F*, a multiple of F, the usual quantity used by crystallographers. F* is proportional to the square root of the intensities. The weight given to each point is not proportional to the statistical error derived above, but one that minimizes the effect of anisotropic extinction. Each value F* (hkl) was assigned a relative weight inversely proportional to the square root of its measured intensity.

$$\sigma_{F^*(hkl)} \propto F^*(hkl) \cdot (Q^{2\theta}(hkl))^{\frac{1}{2}} \qquad \text{(IV-3)}$$

So intense reflections are weighed less than the weak ones, which are less subject to extinction. The results of this procedure are given in table IV-2. The error stated on the parameters is a value that changes the χ^2 by 10%. This is sensible because if the error would have been perfectly estimated, a χ^2 of about 9 would have resulted (Bevington, 1969).

This no-disorder fit will serve as a standard to measure the improvement brought about by allowing for disorder. Because of the relatively good fit obtained without disorder, and because the (111) group of reflections is quite intense, we know that disorder will be quite small. As the number of experimental data is small and there is a relatively large number of parameters to fit, a simple model of

disorder is called for. The model assumes that the disorded atom has the same Debye-Waller factor as the host atom. The masses of the atoms are not strikingly different therefore this is a sensible assumption. This agrees with the results of the no-disorder fit where the Debye-Waller factors are very similar. As a test, the inverse was tried, an atom keeping the same Debye-Waller factor irrespective of the atom site it occupies. The results are substantially the same. This means simply that for atom sites labelled A and B we replace b_A by $(1-t)b_A + tb_B$, and b_B by $(1-t)\ b_B + tb_A$ in the equations II-15 leaving the other terms unaltered. "t" is the chemical disorder between sites A and B, and is a parameter to be fitted. As Webster (1968) stated in his paper one type of disorder tends to be dominant in the Heusler alloys. If we first concentrate on this one, we can afterwards look if a second type of disorder is necessary to explain the data.

The results of this are given in table IV-2, for the type of disorder leading to the largest reduction in χ^2. Note that for all the samples the same type of disorder, Ni $\leftrightarrow$ Mn, tends to be dominant. Bevington (1969) explains how to decide if the improvement in the χ^2 is meaningful, i.e. the pertinence of adding disorder in our model. Form the quantity

$$H = \frac{\chi_N^2 - \chi_M^2}{\chi_M^2}\ M \qquad \text{(IV-4)}$$

where χ_N^2 is the chi-square with the highest number of degrees of freedom, N, and χ_M^2 is a chi-square with M degrees of freedom. H is

Table IV-2: Fitted parameters results

$b_{Ni} = 1.03 \pm .01$ $b_{Sn} = .61 \pm .01$ $b_z = x[-.37 \pm .01] + (1-x)[-.05 \pm .01]$

D.W. factor fitted no disorder allowed	D.W. factor fitted with preferential disorder
<u>x=1.0</u>: $b_z = b_{Mn} = -.37 \pm .01$	
$B_{Ni} = 0.96 \pm .03$	$B_{Ni} = 1.04 \pm .04$
$B_{Sn} = 0.65 \pm .05$	$B_{Sn} = 0.84 \pm .13$
$B_{Mn} = 1.06 \pm .11$	$B_{Mn} = 0.78 \pm .08$
No disorder	$\frac{1}{2}Ni \longleftrightarrow Mn = (3.5 \pm 1.2)\%$
(relative) $\chi^2_9 = 18.9$	$\chi^2_8 = 10.3$ $P(H) = P(6.68) = 5\%$
$R = 1.09$	$R = 0.80$
<u>x=0.8</u>: $b_z = -.31 \pm .01$	
$B_{Ni} = 1.21 \pm .04$	$B_{Ni} = 1.30 \pm .07$
$B_{Sn} = 0.84 \pm .06$	$B_{Sn} = 0.96 \pm .13$
$B_z = 0.82 \pm .13$	$B_z = 0.64 \pm .23$
No disorder	$\frac{1}{2}Ni \longleftrightarrow Mn = (2.0 \pm 2.0)\%$
(relative) $\chi^2_9 = 11.52$	$\chi^2_8 = 10.42$ $P(H) = P(.84) \simeq 42\%$
$R = 1.39$	$R = 1.40$
<u>x=0.6</u>: $b_z = -.24 \pm .01$	
$B_{Ni} = 1.26 \pm .02$	$B_{Ni} = 1.33 \pm .04$
$B_{Sn} = 0.77 \pm .03$	$B_{Sn} = 0.91 \pm .06$
$B_z = 0.99 \pm .10$	$B_z = 0.65 \pm .16$
No disorder	$\frac{1}{2}Ni \longleftrightarrow Mn = (2.8 \pm 0.9)\%$
(relative) $\chi^2_9 = 19.7$	$\chi^2_8 = 10.10$ $P(H) = P(7.60) < 2.5\%$
$R = 0.83$	$R = 0.45$

a well-known tabulated statistical quantity. Using these tables we can find the probability of obtaining a bigger value for H than the one obtained for a reduction by 1 degree of freedom. If this probability is small the change is significant and the disorder is real. The experimental H values are shown in table IV-2 along with their probability.

This shows that only for x=1.0 and x=0.6 is the change significant. A second simultaneous type of disorder does not lead to a significant improvement in χ^2 . The associated probabilities are all higher than 0.5. In addition to the statistical error there is an additional uncertainty caused by the errors in the scattering length. In all cases this causes an additional two (2) percent error in the disorder.

A second independent measure of the goodness of fit, used by crystallographers, is the R factor defined by

$$R = 100 \frac{\sum_{(hkl)} \{F_{obs}(hkl) - F_{calc}(hkl)\}}{\sum_{(hkl)} F_{obs}(hkl)} \qquad \text{(IV-5)}$$

R, even if good by crystallographer's standards, varies quite a bit from sample to sample. The R values increase in the order of, x=0.6, x=1.0 and x=0.8. This can be easily understood if we recall that the crystal cross-sections increase in the same order with extinction being therefore more and more of a problem. Approximating the anisotropic extinction by an isotropic model is less and less

exact. As well the experimental data were collected in the reverse order, i.e. x=0.8 first, x=1.0 second, and x=0.6 last, with greater care taken each time on the orientation of the crystal. The results of all the calculations for each reflections are given in tables A-6, A-7 and are plotted in Fig. IV-2.

Fig. IV-2: ln F* vs $\sin\theta / \lambda$ for structure factor F*

a) x=1.0
. experimental F*
x corrected F*
- calculated F*

(022)

(400)

(422)

(044)

(200)

(2222)

(244)
(600)

(622)

(111)

(311)

(133)

(333)
(511)

(533)

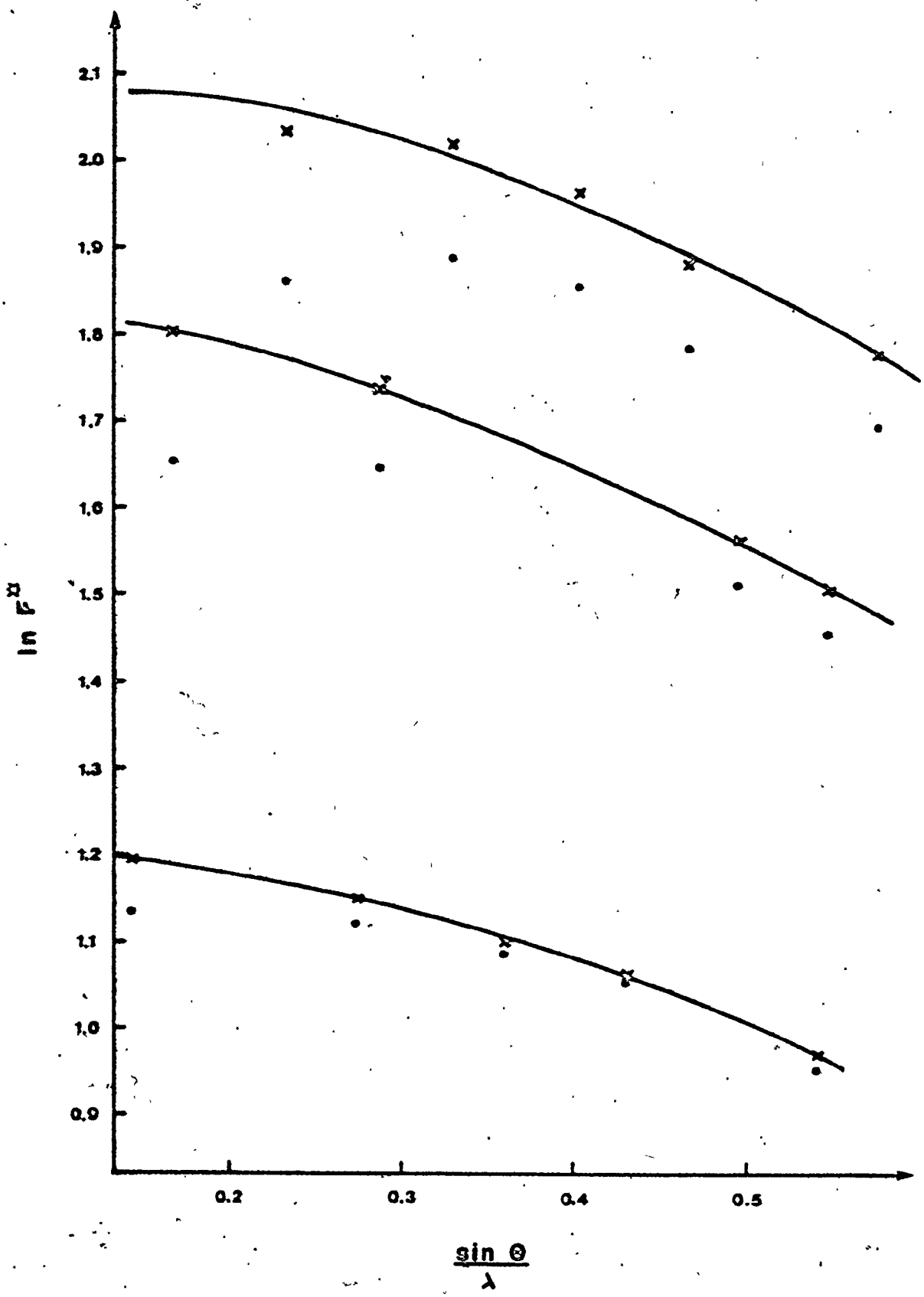
2.1
2.0
1.9
1.8
1.7
1.6
1.5
1.4
1.3
1.2
1.1
1.0
0.9
ln F²
0.2
0.3
0.4
0.5
sin θ / λ

47A

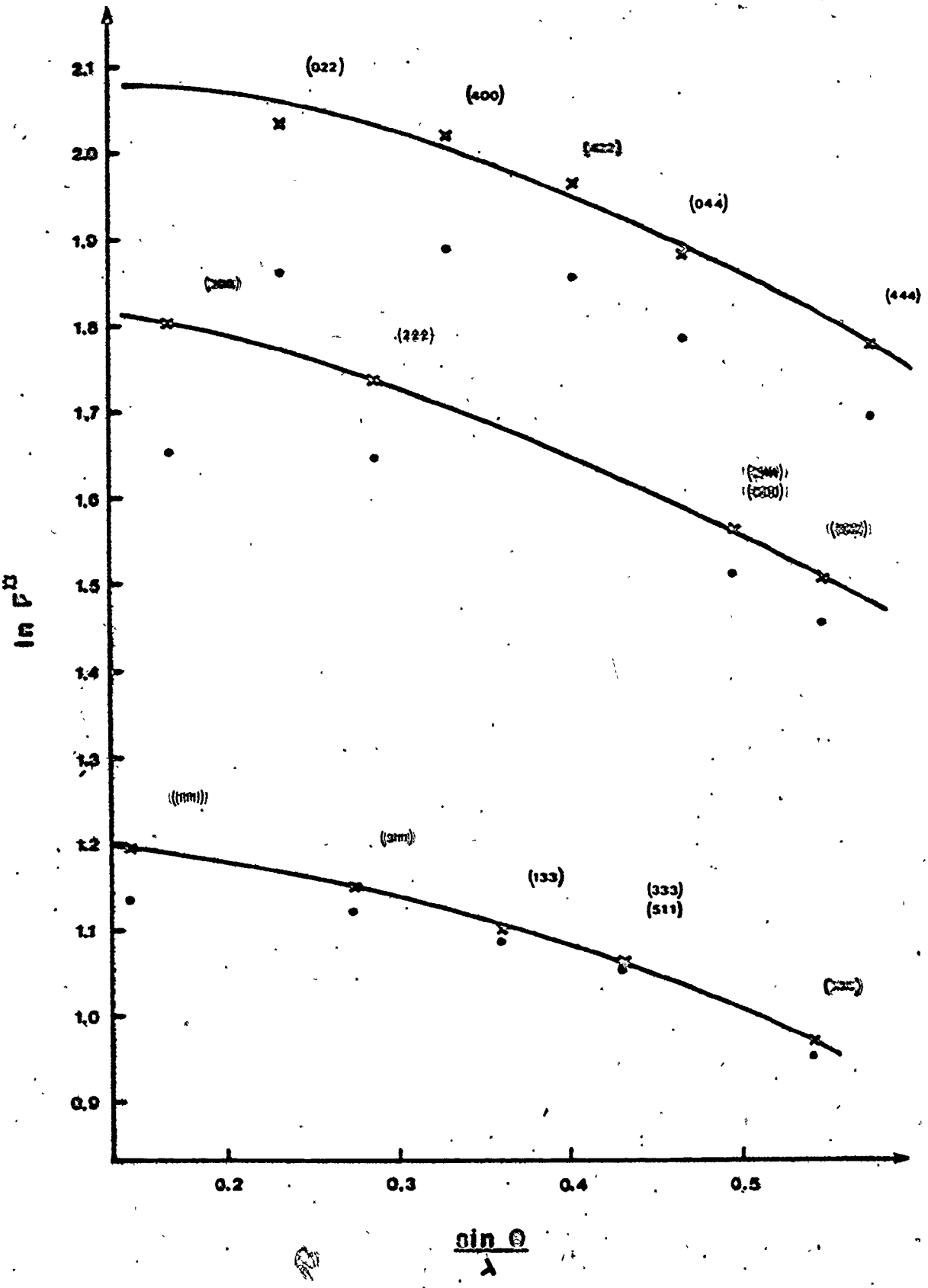
(022)
(400)
(422)
(044)
(444)
(222)
(133)
(333)
(511)
2.1
2.0
1.9
1.8
1.7
1.6
1.5
1.4
1.3
1.2
1.1
1.0
0.9
0.2
0.3
0.4
0.5
ln I^hkl
sin θ / λ

Fig. IV-2: ln F* vs $\sin\theta/\lambda$ for structure factor F*

b) x=0.8
. experimental F*
x corrected F*
- calculated F*

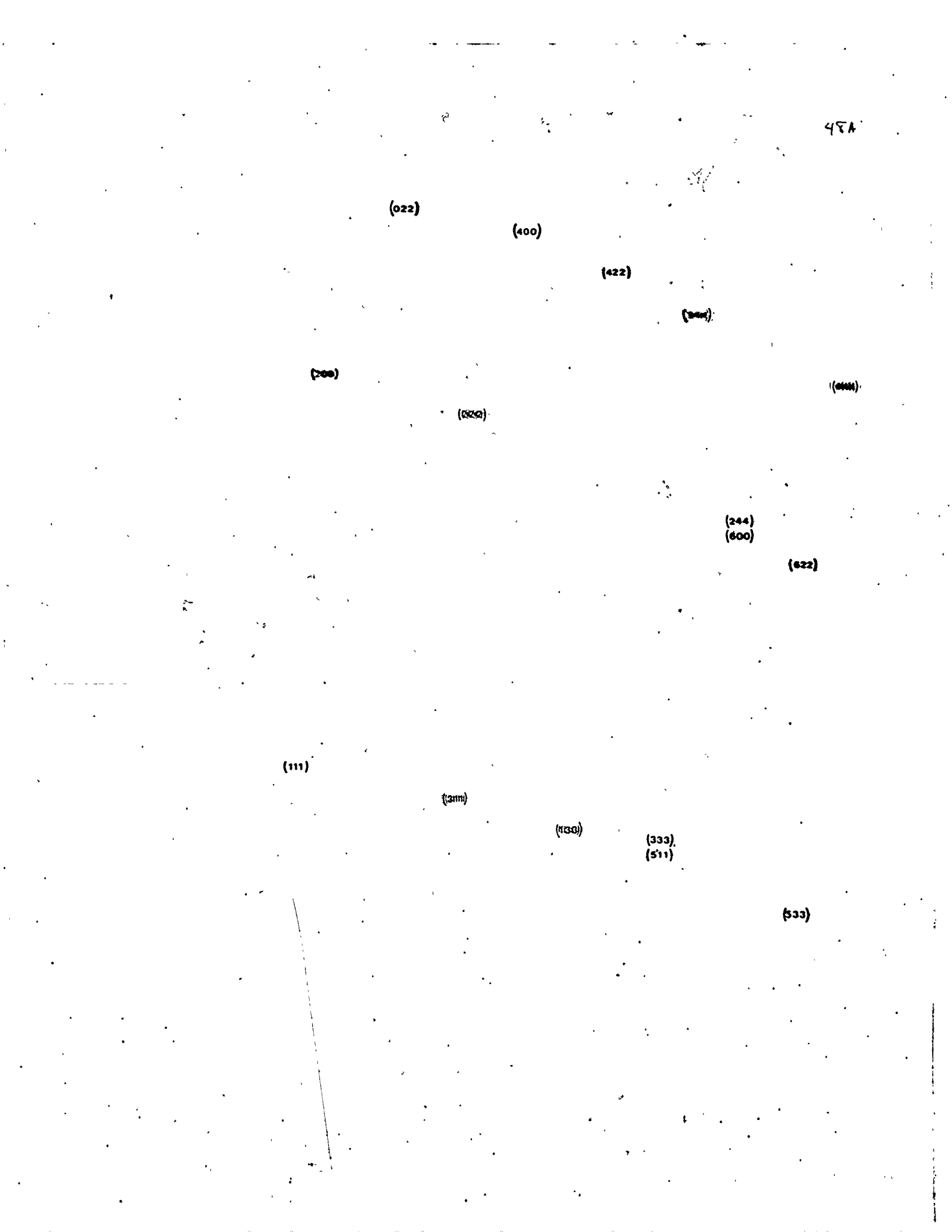
(022)
(400)
(422)
(200)
(244)
(600)
(622)
(111)
(333)
(511)
(533)

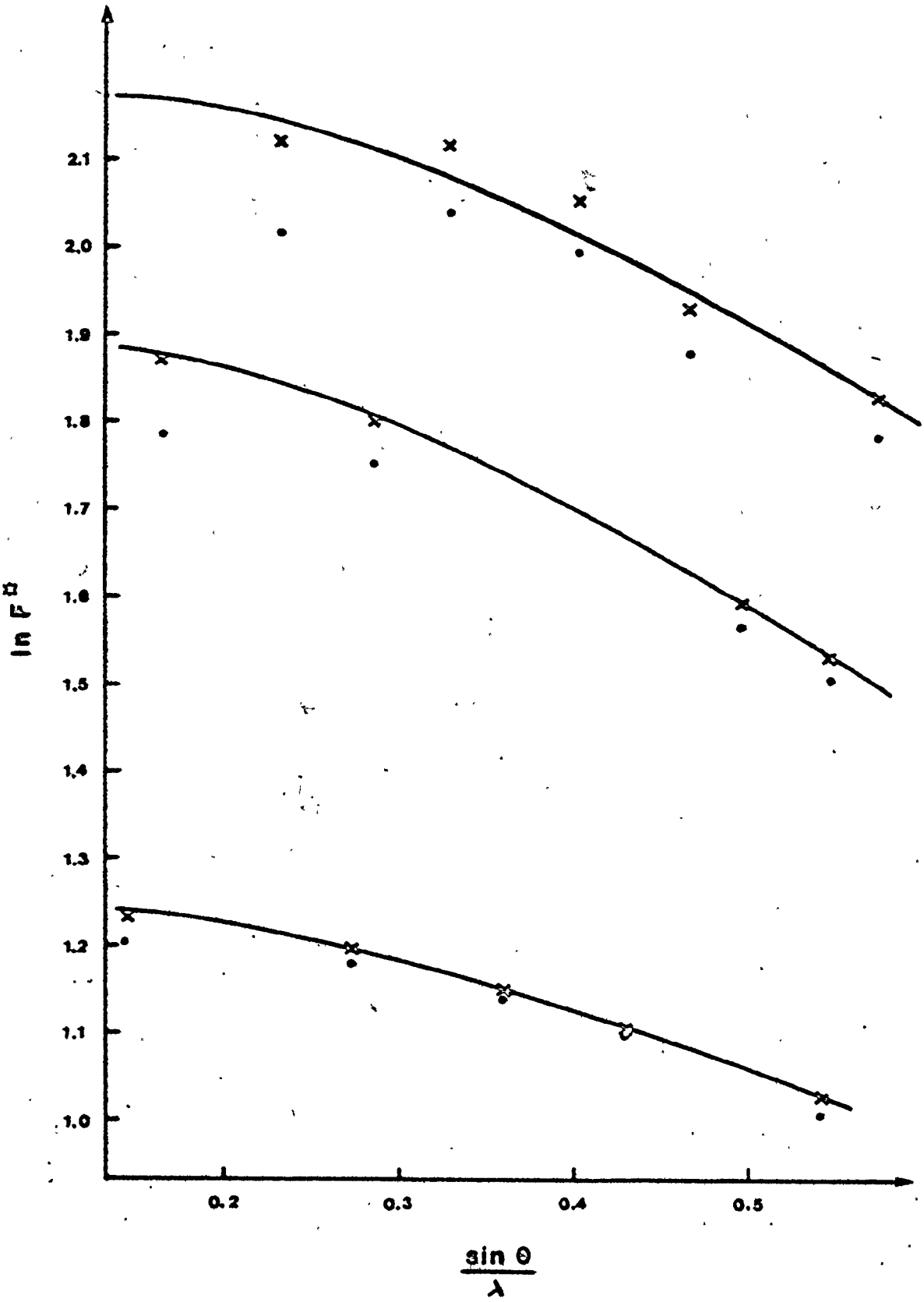
2.1
2.0
1.9
1.8
1.7
1.6
1.5
1.4
1.3
1.2
1.1
1.0
ln F¤
0.2
0.3
0.4
0.5
sin θ / λ

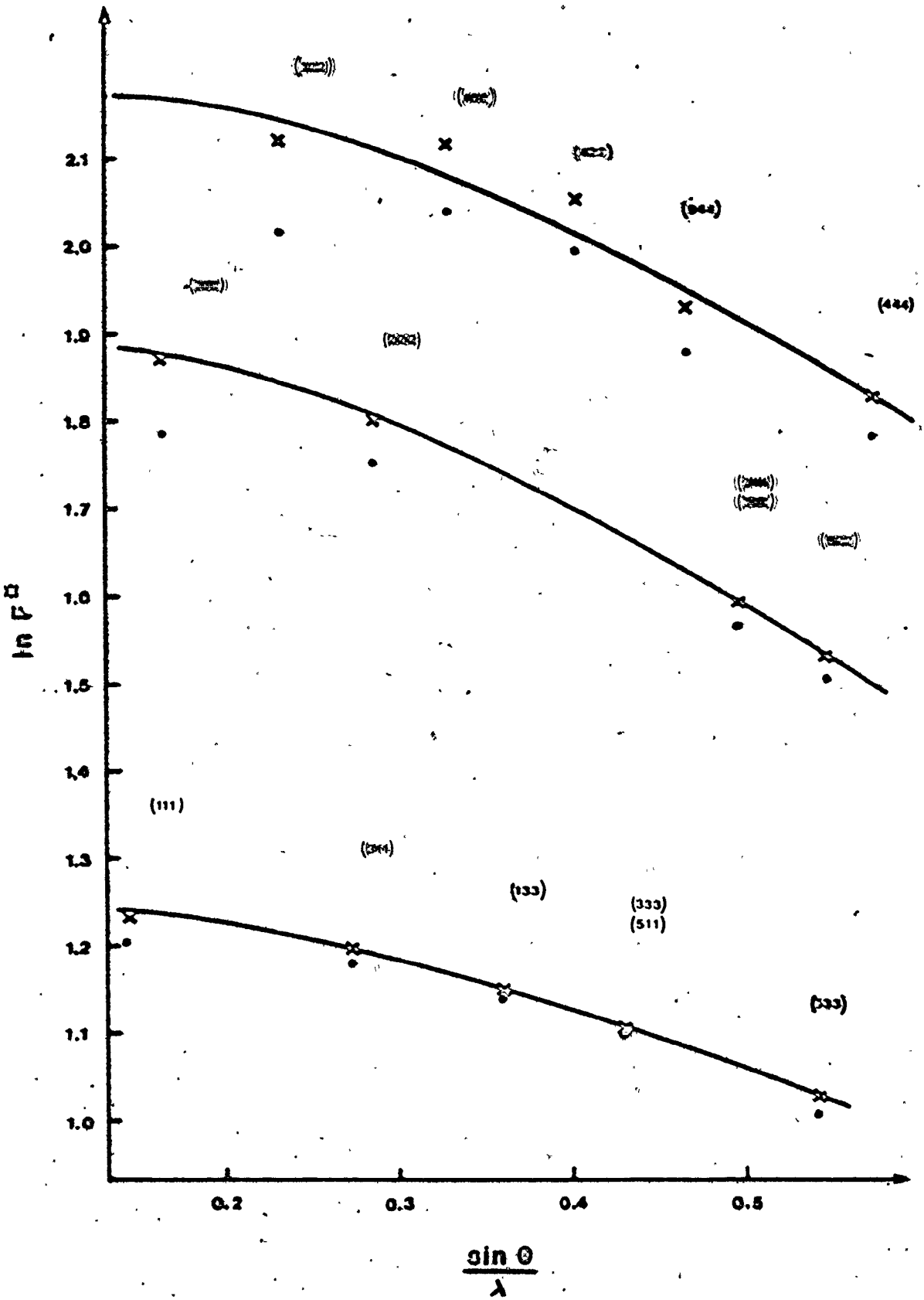
2.1
2.0
1.9
1.8
1.7
1.6
1.5
1.4
1.3
1.2
1.1
1.0
ln F²
(111)
(133)
(333)
(511)
(444)
0.2
0.3
0.4
0.5
sin θ / λ

Fig.-IV-2: ln F* vs $\sin\theta/\lambda$ for structure factor F*

c) x=0.6
. experimental F*
x corrected F*
- calculated F*

49A

(022)

(400)

(422)

(200)

(222)

(244)
(600)

(111)

(311)

(333)
(511)

(533)

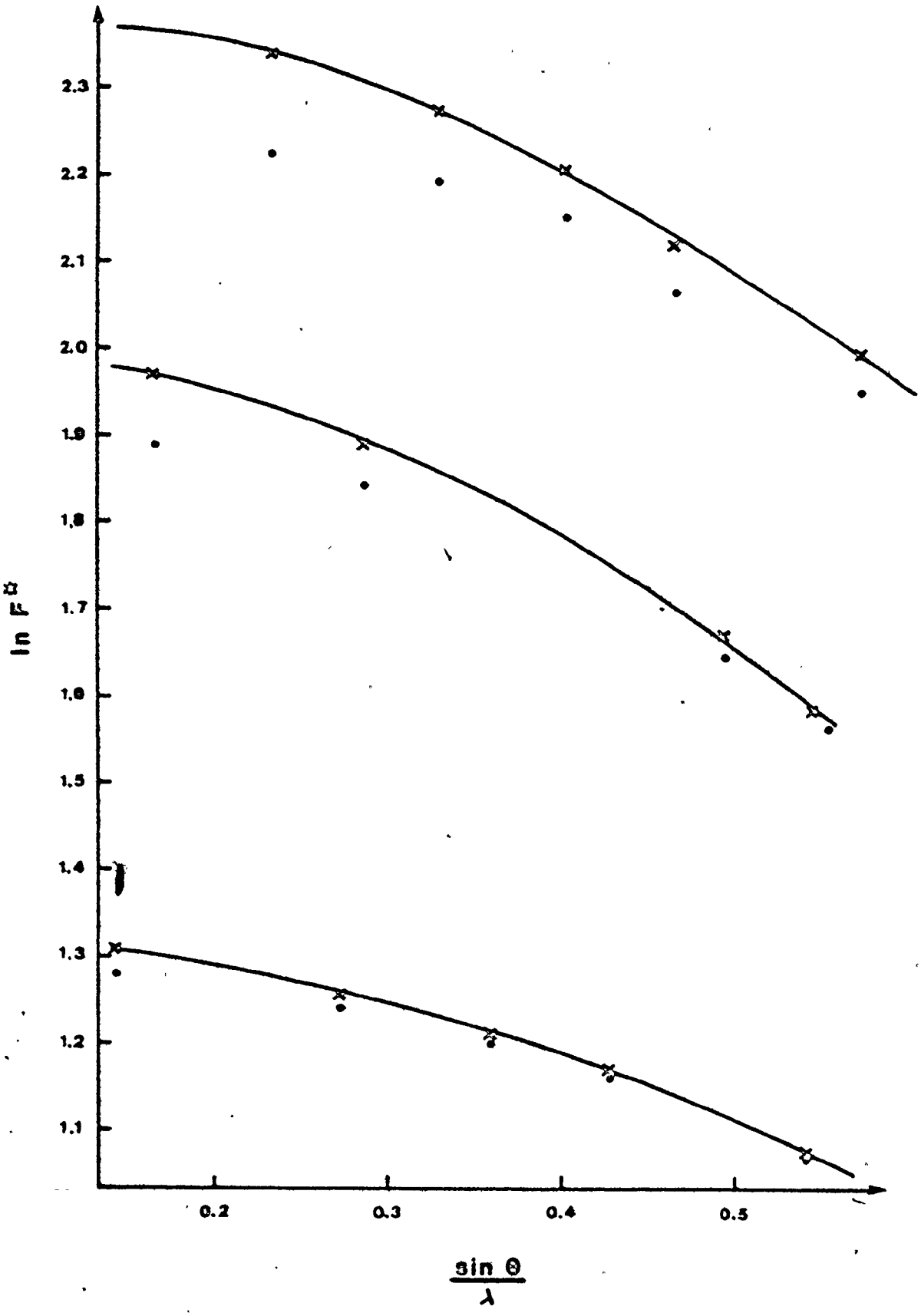
2.3
2.2
2.1
2.0
1.9
1.8
1.7
1.6
1.5
1.4
1.3
1.2
1.1
ln F*
0.2
0.3
0.4
0.5
sin θ / λ

49A

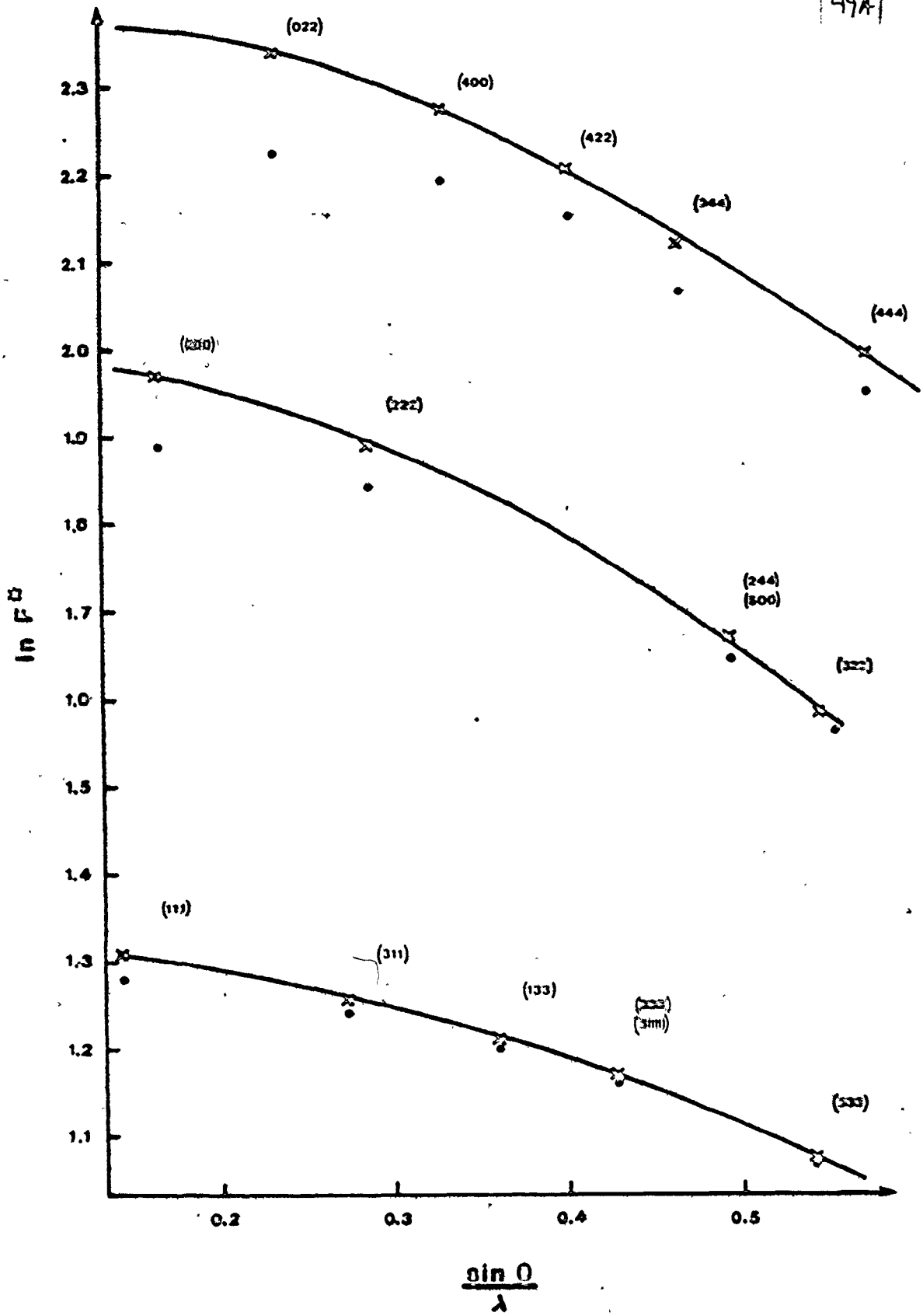
(022)
(400)
(422)
(244)
(444)
(200)
(222)
(244)
(400)
(422)
(111)
(311)
(133)
(333)
2.3
2.2
2.1
2.0
1.9
1.8
1.7
1.6
1.5
1.4
1.3
1.2
1.1
0.2
0.3
0.4
0.5
ln F²
sin θ / λ

CHAPTER V

CONCLUSIONS

The purpose of this work was to accurately measure the chemical order in Heusler alloy single crystals of $Ni_2Mn_xV_{1-x}Sn$, x=1.0, 0.8 and 0.6. These were believed to highly order in the $L2_1$ crystal structure, with Mn and V atoms occupying randomly one of the four FCC sublattices forming the crystal structure.

Neutron diffraction was chosen over x-ray diffraction to measure the chemical ordering. Neutron scattering lengths of Ni, Mn, V and Sn are well apart while Ni, Mn and V x-ray atomic form factors are comparable in size. This makes also the series under study more suitable for chemical disorder measurements than previous studies on Pd_2MnX, where X stands for Sn, Sb or In. For all X, Pd and X are very difficult to differentiate with both neutrons and x-rays.

Long thin crystals were cut by spark erosion from large single crystal boules grown by Kyropoulos or Bridgman method. The crystal cross-sections were less than 1 mm. The data of the diffraction could not be made extinction free. Therefore, they were corrected numerically. The structure factors were calculated by an iterative method minimizing the χ^2, allowing for different types of disorder to

occur. The variation in χ^2 served as discriminator to determine the best fit, as opposed to the absolute value of χ^2.

The results confirm that they all highly ordered. It is not necessary to introduce any disorder to explain the data for x=0.8 sample. A slight DO_3 disorder (V,Mn $\leftrightarrow$ Ni) is sufficient to explain the data for the x=1.0 and x=0.6 samples: (3.5±1.2) % of (V,Mn) atoms disorder with Ni in x=1.0, and (2.8 ± 0.9) % of (V,Mn) atoms in x=0.6. No B2 disorder (V, Mn $\leftrightarrow$ Sn) nor DO_3 of type (Ni $\leftrightarrow$ Sn) are necessary to explain the data. These results are similar to those of Webster (1967) on Pd_2MnSn and differ strongly with Birchall et al (1980 a, b) conclusions on polycrystalline samples of the same series under study in this work.

APPENDIX

Table A-1: Structure factors for Ni_2MnSn and Nuclear Scattering length

$b_{Ni} = 1.03 \times 10^{-12}$cm

$b_{Mn} = -0.37 \times 10^{-12}$cm

$b_{V} = -0.05 \times 10^{-12}$cm

$b_{Sn} = 0.61 \times 10^{-12}$cm

hkl	$f(\vec{G})$	$\lvert F_M \rvert^2$ ($\times 10^{-24}$cm^2)	$\lvert F_N \rvert^2$ ($\times 10^{-24}$cm^2)	$\frac{2}{3}\frac{\lvert F_M \rvert^2}{\lvert F_{Tot} \rvert^2}$ (%)
111	0.794 ± .005	3.66 ± .05	15.37	13.7
200	0.741	3.18 .04	53.00	3.8
220	0.557	1.80 .03	84.64	1.4
311	0.464	1.25 .03	15.37	5.1
222	0.423	1.03 .02	53.00	1.3
400	0.353	0.72 .02	84.64	0.6
331	0.297	0.51 .02	15.37	2.2
422	0.233	0.31 .01	84.64	0.3
333	0.198	0.23 .01	15.37	1.0
511	0.198	0.23 .01	15.37	1.0
044	0.153	0.14 .01	84.64	0.1
244	0.123	0.088 .007	53.00	0.1
600	0.123	0.088 .007	53.00	0.1
533	0.092	0.048 .005	15.37	0.2
622	0.083	0.040 .005	53.00	0.0
444	0.069	0.028 .004	84.64	0.0

Tables A-2: Bragg intensities for λ = 1.47 Å

a) x = 1.: Ni_2MnSn, λ = 1.472 Å

Normalized monitor count to 50,000

(hkl)	2θ	I	± ΔI	(hkl)	2θ	I	± ΔI
111	24.28°	24745	± 190	$\bar{3}33$	78.25°	7763	± 57
$\bar{1}\bar{1}1$		25463	193	$\bar{3}\bar{3}3$		7645	56
$\bar{1}\bar{1}\bar{1}$		25191	194	$\bar{3}\bar{3}\bar{3}$		7815	57
$1\bar{1}\bar{1}$		25816	195	$3\bar{3}\bar{3}$		7790	57
200	28.11°	55733	398	511	78.25°	7639	56
$\bar{2}00$		55208	398	$\bar{5}11$		7615	57
				$\bar{5}\bar{1}1$		7684	57
022	40.18°	60421	293	$5\bar{1}1$		7531	56
$0\bar{2}\bar{2}$		58209	288				
				044	86.78°	32813	135
311	47.50°	12398	85	$0\bar{4}\bar{4}$		32377	134
$\bar{3}11$		12330	88				
$3\bar{1}\bar{1}$		12297	87	244	93.54°	19054	104
$3\bar{1}\bar{1}$		12567	88	$\bar{2}44$		18603	102
				$\bar{2}\bar{4}\bar{4}$		19457	105
222	49.75°	31989	211	$2\bar{4}\bar{4}$		18776	103
$\bar{2}\bar{2}2$		32940	214				
$\bar{2}\bar{2}\bar{2}$		33133	215	600	93.54°	18523	103
				$\bar{6}00$		18755	103
400	58.12°	47200	228				
$\bar{4}00$		47489	229	533	105.56°	6464	40
				$\bar{5}33$		6474	41
133	63.92°	9205	63	$\bar{5}\bar{3}3$		6568	41
$\bar{1}33$		8971	63	$5\bar{3}3$		6471	41
$\bar{1}\bar{3}\bar{3}$		9027	62				
$1\bar{3}\bar{3}$		9150	63	622	107.32°	17321	99
				$\bar{6}22$		17610	101
422	73.01°	38121	146	$\bar{6}\bar{2}2$		17714	101
$\bar{4}22$		39879	150	$6\bar{2}2$		17974	102
$\bar{4}\bar{2}\bar{2}$		39015	147				
$4\bar{2}\bar{2}$		39367	149	444	114.57°	29614	128
				$\bar{4}44$		29700	129
				$\bar{4}\bar{4}4$		29211	128
				$4\bar{4}4$		29999	129

Tables A-2: Bragg intensities for $\lambda = 1.47$ Å (cont'd)

b) x=0.8: $Ni_2Mn_{.8}V_{.2}Sn$, $\lambda = 1.470$ Å

Normalized monitor count to 50,000

(hkl)	2θ	I	± ΔI	(hkl)	2θ	I	± ΔI
111	24.26°	24888	± 121	333	78.14°	8502	± 58
$1\bar{1}\bar{1}$		25186	121	$3\bar{3}\bar{3}$		8186	57
$\bar{1}\bar{1}\bar{1}$		25122	121	$\bar{3}\bar{3}\bar{3}$		8316	58
				$\bar{3}33$		8955	59
200	28.08°	70210	281				
$\bar{2}00$		68039	277	$51\bar{1}$	78.14°	8249	56
				$5\bar{1}\bar{1}$		8396	58
022	40.14°	80904	302	$\bar{5}\bar{1}\bar{1}$		8640	58
$0\bar{2}\bar{2}$		78227	296	$\bar{5}11$		8761	59
311	47.44°	13358	71	044	86.66°	42163	176
$3\bar{1}\bar{1}$		13022	71	$0\bar{4}\bar{4}$		36006	162
$\bar{3}1\bar{1}$		13642	73				
$\bar{3}11$		13576	72	244	93.40°	22024	90
				$2\bar{4}\bar{4}$		19083	84
222	49.70°	39969	171	$\bar{2}4\bar{4}$		20116	86
$2\bar{2}\bar{2}$		39114	169	$\bar{2}44$		22835	91
$\bar{2}2\bar{2}$		40148	172				
$\bar{2}22$		40819	173	600	93.40°	20055	86
				$\bar{6}00$		22085	90
400	58.06°	61400	259				
$\bar{4}00$		65599	269	533	105.40°	7034	35
				$5\bar{3}\bar{3}$		6634	35
133	63.84°	10351	55	$\bar{5}3\bar{3}$		7208	36
$1\bar{3}\bar{3}$		9620	53	$\bar{5}33$		7825	38
$\bar{1}3\bar{3}$		9945	54				
$\bar{1}33$		10368	55	622	107.14°	18163	101
				$6\bar{2}\bar{2}$		18459	101
422	72.92°	50761	192	$\bar{6}2\bar{2}$		19727	105
$4\bar{2}\bar{2}$		49723	190	$\bar{6}22$		21206	109
$\bar{4}2\bar{2}$		51776	195				
$\bar{4}22$		53472	198	444	114.36°	36246	163
				$4\bar{4}\bar{4}$		30694	149
				$\bar{4}4\bar{4}$		35520	160
				$\bar{4}44$		38796	168

Tables A-2: Bragg intensities for λ = 1.47 Å (cont'd)

c) x=0.6: $Ni_2Mn_{.6}V_{.4}Sn$, λ = 1.468 Å

Normalized monitor count to 50,000

(hkl)	2θ	I	±	ΔI	(hkl)	2θ	I	±	ΔI
111	24.23°	28747	±	170	333	78.06°	9682	±	79
$\bar{1}11$		29428		172	$\bar{3}33$		9456		78
$\bar{1}\bar{1}\bar{1}$		29280		175	$\bar{3}\bar{3}\bar{3}$		10125		80
$1\bar{1}\bar{1}$		29973		175	$3\bar{3}\bar{3}$		9531		78
200	28.05°	85262		498	511	78.06°	9566		78
$\bar{2}00$		85975		503	$\bar{5}11$		9645		78
					$\bar{5}\bar{1}\bar{1}$		9849		79
022	40.09°	120180		683	$5\bar{1}\bar{1}$		9636		79
$0\bar{2}\bar{2}$		122170		693					
					044	86.56°	55893		393
311	47.40°	15173		89	$0\bar{4}\bar{4}$		57395		400
$\bar{3}11$		15169		88					
$\bar{3}\bar{1}\bar{1}$		15078		88	$2\bar{4}\bar{4}$	93.29°	24680		118
$3\bar{1}\bar{1}$		15152		88	$\bar{2}44$		24150		117
					$\bar{2}\bar{4}\bar{4}$		25341		120
222	49.65°	46485		360	$2\bar{4}\bar{4}$		24517		118
$\bar{2}22$		48648		368					
$\bar{2}\bar{2}\bar{2}$		48423		370	600	93.29°	24902		119
$2\bar{2}\bar{2}$		48350		368	$\bar{6}00$		24644		118
400	57.99°	86020		495	533	105.25°	8112		59
$\bar{4}00$		86338		495	$\bar{5}33$		8151		59
					$\bar{5}\bar{3}\bar{3}$		8336		60
133	63.77°	11194		68	$5\bar{3}\bar{3}$		7950		58
$\bar{1}33$		11228		67					
$\bar{1}\bar{3}\bar{3}$		11723		69	622	107.00°	21701		143
$1\bar{3}\bar{3}$		11612		68	$\bar{6}22$		21753		145
					$\bar{6}\bar{2}\bar{2}$		21803		144
422	72.84°	69317		507	$6\bar{2}\bar{2}$		21836		144
$\bar{4}22$		70133		510					
$\bar{4}\bar{2}\bar{2}$		68000		503	444	114.20°	48514		326
$4\bar{2}\bar{2}$		71387		517	$\bar{4}44$		50502		236
					$\bar{4}\bar{4}\bar{4}$		49166		332
					$4\bar{4}\bar{4}$		47844		324

Tables A-3: Bragg intensities by symmetry related reflections for $\lambda = 1.47$ Å

a) (averaged over symmetry related reflections, corrected for Lorentz factor, $\lambda/2$ contamination and magnetic scattering)

x = 1.: Ni_2MnSn, $\lambda = 1.472$ Å

Normalized to 50,000 monitor counts

(hkl)	$\left(\frac{\sin\theta}{\lambda}\right)^2$	Io=I* sin 2θ	lnIo
111	.0204	8707 ± 34	9.072 ± .004
311	.0749	8424 30	9.039 .004
133	.1293	7759 27	8.957 .003
511	.1838	7177 27	8.879 .004
333	.1838	7305 27	8.896 .004
533	.2927	6069 19	8.711 .003
200	.0272	24701 126	10.115 .005
222	.0817	24255 93	10.096 .004
244	.2450	18667 51	9.834 .003
600	.2450	18339 73	9.817 .004
622	.2995	16611 49	9.718 .003
022	.0545	37319 130	10.527 .004
400	.1089	39574 135	10.586 .003
422	.1633	36937 71	10.517 .002
044	.2178	32203 94	10.380 .003
444	.3267	26694 59	10.192 .002

Tables A-3: Bragg intensities by symmetry related reflections for $\lambda = 1.47$ Å

b) (averaged over symmetry related reflections, corrected for $\lambda/2$ contamination and for Lorentz factor)

x=0.8: $Ni_2Mn_{.8}V_{.2}Sn$, $\lambda = 1.470$ Å

Normalized to 50,000 monitor counts

(hkl)	$\left(\frac{\sin\theta}{\lambda}\right)^2$	Io=I* sin 2θ	lnIo
111	.0204	9986 ± 29	9.209 ± .003
311	.0749	9579 30	9.167 .003
133	.1294	8776 24	9.080 .003
511	.1838	8088 28	8.998 .003
333	.1838	8068 28	8.996 .003
533	.2928	6717 17	8.813 .003
200	.0272	31986 93	10.373 .003
222	.0817	29890 65	10.305 .002
244	.2451	20657 44	9.936 .002
600	.2451	20713 62	9.938 .003
622	.2996	18255 50	9.812 .003
022	.0545	50814 136	10.836 .003
400	.1090	53397 158	10.886 .003
422	.1634	48490 93	10.789 .002
044	.2179	38489 117	10.558 .003
444	.3268	31739 72	10.365 .002

Tables A-3: Bragg intensities by symmetry related reflections for $\lambda = 1.47$ Å

c) (averaged over symmetry related reflections, corrected for $\lambda/2$ contamination and for Lorentz factor)

x=0.6: $Ni_2Mn_{.6}V_{.4}Sn$, $\lambda = 1.467$ Å

Normalized to 50,000 monitor counts

(hkl)	$\left(\frac{\sin\theta}{\lambda}\right)^2$	Io=I* sin 2θ	lnIo
111	.0204	11701 ± 35	9.368 ± .003
311	.0750	10796 51	9.287 .005
133	.1295	9940 30	9.204 .003
511	.1840	9169 38	9.124 .004
333	.1840	9193 39	9.126 .004
533	.2930	7606 29	8.937 .004
200	.0273	39493 166	10.584 .004
222	.0818	35916 139	10.489 .004
244	.2453	24201 59	10.094 .002
600	.2453	24299 84	10.098 .003
622	.2999	20473 69	9.927 .003
022	.0545	77267 314	11.255 .004
400	.1090	72406 295	11.190 .004
422	.1636	66016 242	11.098 .004
044	.2181	56052 277	10.934 .005
444	.3271	44320 133	10.699 .003

Tables A-4: Bragg intensities for a second wavelength, λ = 1.03 Å

a) x=1.0: Ni_2MnSn, λ = 1.033 Å

Normalized to 50,000 monitor counts

(hkl)	2θ	I	± ΔI	(hkl)	2θ	I	± ΔI
111	16.98°	10366	± 92	400	39.86°	20215	± 134
$\bar{1}11$		10089	85	$\bar{4}00$		18734	131
$\bar{1}\bar{1}\bar{1}$		10292	93				
$1\bar{1}1$		11500	92	422	49.36°	15250	87
				$\bar{4}22$		15137	89
200	19.62°	25857	176	$\bar{4}\bar{2}\bar{2}$		15598	88
$\bar{2}00$		23416	168	$4\bar{2}\bar{2}$		16983	93
022	27.90°	26681	196	044	57.64°	11958	77
$0\bar{2}\bar{2}$		28171	144	$0\bar{4}\bar{4}$		13157	80
222	34.34°	13451	101	444	72.38°	8951	70
$\bar{2}22$		12996	99	$\bar{4}44$		9071	70
$\bar{2}\bar{2}\bar{2}$		14146	104	$\bar{4}\bar{4}\bar{4}$		9823	73
$2\bar{2}\bar{2}$		14754	105	$4\bar{4}\bar{4}$		10350	74

Tables A-4: Bragg intensities for a second wavelength, $\lambda = 1.03$ Å

b) x=0.8: $Ni_2Mn_{.8}V_{.2}Sn$, $\lambda = 1.035$ Å

Normalized to 50,000 monitor counts

(hkl)	2θ	I	± ΔI	(hkl)	2θ	I	± ΔI
111	17.01°	11840	± 95	422	49.46°	22349	± 159
$\bar{1}11$		12438	98	$\bar{4}22$		24340	167
$\bar{1}\bar{1}\bar{1}$		12186	96	$\bar{4}\bar{2}\bar{2}$		24125	164
$1\bar{1}\bar{1}$		11712	95	$4\bar{2}\bar{2}$		21879	158
200	19.67°	33383	223	044	57.77°	18882	147
$\bar{2}00$		36454	233	$0\bar{4}\bar{4}$		16766	139
022	27.95°	43050	246	600	61.64°	8226	54
$0\bar{2}\bar{2}$		41086	241	$\bar{6}00$		9236	56
311	32.91°	5954	44	244	61.64°	8792	55
$\bar{3}11$		6544	48	$\bar{2}44$		9203	56
$\bar{3}\bar{1}\bar{1}$		6489	46	$\bar{2}\bar{4}\bar{4}$		8199	54
$3\bar{1}\bar{1}$		5850	47	$2\bar{4}\bar{4}$		8515	52
222	34.41°	18749	104	444	72.55°	12756	84
$\bar{2}22$		19568	107	$\bar{4}44$		14023	87
$\bar{2}\bar{2}\bar{2}$		19535	107	$\bar{4}\bar{4}\bar{4}$		12453	83
$2\bar{2}\bar{2}$		18170	103	$4\bar{4}\bar{4}$		11395	80
400	39.95°	28108	177				
$\bar{4}00$		31629	188				

Tables A-4: Bragg intensities for a second wavelength, $\lambda = 1.03$ Å

c) x=0.6: $Ni_2Mn_{.6}V_{.4}Sn$, $\lambda = 1.027$ Å

Normalized to 50,000 monitor counts

(hkl)	2θ	I	±	ΔI	(hkl)	2θ	I	±	ΔI
111	16.88°	10099	±	72	400	39.64°	28252	±	168
$\bar{1}11$		9443		71	$\bar{4}00$		30767		176
$1\bar{1}1$		10753		74					
$11\bar{1}$		10564		73	422	49.08°	23686		236
					$\bar{4}22$		22960		234
200	19.52°	29632		177	$\bar{4}\bar{2}\bar{2}$		21488		226
$\bar{2}00$		32680		186	$4\bar{2}\bar{2}$		22980		234
022	27.74°	42100		254	044	57.32°	17450		173
$0\bar{2}\bar{2}$		46915		268	$0\bar{4}\bar{4}$		18387		177
222	34.16°	15917		167	444	71.94°	12423		114
$\bar{2}22$		16177		167	$\bar{4}44$		12538		115
$\bar{2}\bar{2}\bar{2}$		17101		170	$\bar{4}\bar{4}\bar{4}$		13391		117
$2\bar{2}\bar{2}$		16349		169	$4\bar{4}\bar{4}$		12778		115

Tables A-5: Bragg intensities by symmetry related reflections, λ = 1.03 Å

a) (Averaged over symmetry related reflections, corrected for magnetic scattering, and for Lorentz factor)

x=1.0: Ni_2MnSn, λ = 1.033 Å

** Normalized to (hkl = 222) of (λ = 1.47 Å)

(hkl)	$\left(\frac{\sin\theta}{\lambda}\right)^2$	Io=I* sin 2 θ	lnIo
111	.0204	8379 ± 36	9.033 ± .004
200	.0272	25039 126	10.128 .005
222**	.0817	24255 60	10.096 .003
022	.0545	39832 171	10.592 .004
400	.1089	39067 191	10.573 .005
422	.1633	37503 109	10.532 .003
044	.2178	33351 151	10.415 .005
444	.3267	28639 109	10.262 .004

Tables A-5: Bragg intensities by symmetry related reflections, λ = 1.03 Å,

b) (Averaged over symmetry related reflections, corrected for the Lorentz factor)

x=0.8: $Ni_2Mn_{.8}V_{.2}Sn$, λ = 1.035 Å

** Normalized to (hkl = 222) of (λ = 1.47 Å)

(hkl)	$\left(\frac{\sin\theta}{\lambda}\right)^2$	Io=I* sin 2θ		inIo	
111	.0204	9801	± 40	9.190	± .004
311	.0749	9386	35	9.147	.004
200	.0272	32701	152	10.395	.005
222**	.0817	29890	85	10.305	.003
600	.2451	21377	97	9.969	.005
244	.2451	21247	67	9.963	.003
022	.0545	54866	228	10.913	.004
400	.1090	53363	233	10.885	.004
422	.1634	49004	174	10.800	.004
044	.2179	41959	242	10.645	.006
444	.3268	33603	109	10.423	.003

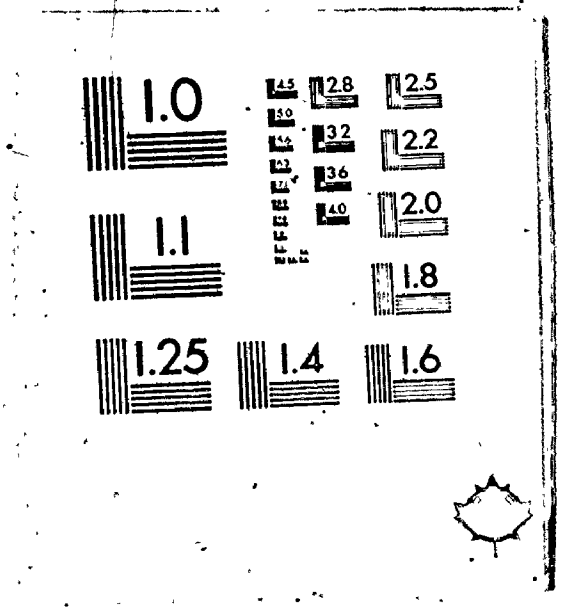

Tables A-5: Bragg intensities by symmetry related reflections, λ = 1.03 Å

c) (Averaged over symmetry related reflections, corrected for the Lorentz factor)

x=0.6: $Ni_2Mn_{.6}V_{.4}Sn$, λ = 1.027 Å

** Normalized to (hkl = 222) of (λ = 1.47 Å)

(hkl)	$\left(\frac{\sin\theta}{\lambda}\right)^2$	Io=I* sin 2θ	lnIo
111	.0204	11578 ± 42	9.357 ± .004
200	.0273	40638 169	10.612 .004
222**	.0818	35916 187	10.489 .005
022	.0545	80869 340	11.301 .004
400	.1090	73486 310	11.205 .004
422	.1636	67188 348	11.115 .005
044	.2181	58873 414	10.983 .007
444	.3271	47440 219	10.767 .005

Tables A-6: Relative F values for each reflection for the best fit

a) x=1.0

(hkl)	Fexp	Fcorr	Fcalc	$100\left(\frac{Fcorr - Fcalc}{Fcorr}\right)$	y(hkl)
111	3.1103	3.3072	3.3049	.1	.884
311	3.0595	3.1628	3.1609	.1	.936
133	2.9362	3.0115	3.0232	- .4	.951
511	2.8365	2.8979	2.8915	.2	.958
333					
533	2.5968	2.6449	2.6450	- .0	.964
200	5.2388	6.0773	6.0383	.6	.743
222	5.1913	5.6925	5.6980	- .1	.832
600	4.5342	4.7854	4.7876	- .0	.898
244					
622	4.2961	4.5189	4.5176	.0	.904
022	6.4394	7.6582	7.8478	-2.5	.707
400	6.6310	7.5493	7.4226	1.7	.772
422	6.4063	7.1367	7.0205	1.6	.806
044	5.9817	6.5786	6.6402	- .9	.827
444	5.4461	5.9313	5.9403	- .2	.843

B_{Ni} = 1.04 ± .04

B_{Sn} = 0.84 ± .13

B_{Mn} = 0.78 ± .08

Disorder: Ni ⟷ Mn: (3.5 ± 1.2) at. %

χ^2_8 = 10.3 (relative)

R = 0.80

P (H) = P (6.68) < 5%

Tables A-6: Relative F values for each reflection for the best fit

b) x=0.8

(hkl)	Fexp	Fcorr	Fcalc	$100\left(\frac{Fcorr - Fcalc}{Fcorr}\right)$	y(hkl)
111	3.3310	3.4374	3.4636	- .8	.939
311	3.2625	3.3168	3.3096	.2	.968
133	3.1227	3.1619	3.1625	- .0	.975
333	2.9959	3.0275	3.0220	.2	.979
511					
533	2.7320	2.7564	2.7593	- .1	.982
200	5.9615	6.5020	6.5232	- .3	.841
222	5.7629	6.0602	6.0848	- .4	.904
600	4.7941	4.9231	4.9362	- .3	.948
244					
622	4.5037	4.6142	4.6029	.2	.953
022	7.5140	8.3413	8.5324	-2.3	.811
400	7.7026	8.2980	8.0072	3.5	.862
422	7.3401	7.7940	7.5147	3.6	.887
044	6.5395	6.8851	7.0528	-2.4	.902
444	5.9385	6.2083	6.2133	- .1	.915

$B_{Ni} = 1.21 \pm .04$

$B_{Sn} = 0.84 \pm .06$

$B_z = 0.82 \pm .13$

No Disorder

$\chi^2_9 = 11.52$ (relative)

$R = 1.39$

Tables A-6: Relative F values for each reflection for the best fit

c) x=0.6

(hkl)	Fexp	Fcorr	Fcalc	$100\left(\frac{Fcorr - Fcalc}{Fcorr}\right)$	y(hkl)
111	3.6058	3.7041	3.6887	.4	.948
311	3.4634	3.5124	3.5226	- .3	.972
133	3.3234	3.3588	3.3642	- .2	.979
333	3.1939	3.2224	3.2130	.3	.982
511					
533	2.9071	2.9290	2.9311	- .1	.985
200	6.6243	7.1729	7.1708	.0	.853
222	6.3171	6.6095	6.6419	- .5	.913
600	5.1908	5.3106	5.2770	.6	.955
244					
622	4.7694	4.8683	4.8872	- .4	.960
022	9.2657	10.3820	10.4051	- .2	.797
400	8.9695	9.7221	9.7001	.2	.851
422	8.5646	9.1334	9.0429	1.0	.879
044	7.8918	8.3345	8.4302	-1.1	.897
444	7.0175	7.3473	7.3266	.3	.912

B_{Ni} = 1.33 ±.04

B_{Sn} = 0.91 ±.06

B_z = 0.65 ±.16

Disorder: Ni⟷Mn = (2.8 ± .9) at., %

X_8^2 = 10.1 (relative)

R = 0.45

P (H) = P (7.60) < 2.5%

Tables A-7: Logarithm for the best fit

a) x=1.0

(hkl)	ln Fexp	ln Fcorr	ln Fcalc	sinθ/λ
111	1.1347	1.1961	1.1954	.143
311	1.1183	1.1515	1.1509	.274
133	1.0771	1.1024	1.1063	.360
511	1.0426	1.0640	1.0618	.429
333				
533	.9543	.9726	.9727	.541
200	1.6561	1.8046	1.7981	.165
222	1.6470	1.7391	1.7401	.286
600	1.5116	1.5656	1.5660	.495
244				
622	1.4577	1.5083	1.5080	.547
022	1.8624	2.0358	2.0602	.233
400	1.8918	2.0215	2.0045	.330
422	1.8573	1.9653	1.9488	.404
044	1.7887	1.8838	1.8931	.467
444	1.6949	1.7802	1.7818	.572

Tables A-7: Logarithm for the best fit

b) x=0.8

(hkl)	ln Fexp	ln Fcorr	ln Fcalc	sin θ/λ
111	1.2033	1.2347	1.2423	.143
311	1.1825	1.1990	1.1968	.274
133	1.1387	1.1512	1.1514	.360
511	1.0972	1.1077	1.1059	.429
333				
533	1.0050	1.0139	1.0150	.541
200	1.7853	1.8721	1.8754	.165
222	1.7514	1.8017	1.8058	.286
600	1.5674	1.5939	1.5966	.495
244				
622	1.5049	1.5291	1.5267	.547
022	2.0168	2.1212	2.1439	.233
400	2.0416	2.1160	2.0803	.330
422	1.9934	2.0534	2.0169	.404
044	1.8779	1.9294	1.9534	.467
444	1.7815	1.8259	1.8267	.572

Tables A-7: Logarithm for the best fit

c) x=0.6

(hkl)	ln Fexp	ln Fcorr	ln Fcalc	sinθ/λ
111	1.2825	1.3094	1.3053	.143
311	1.2423	1.2563	1.2592	.274
133	1.2010	1.2116	1.2132	.360
511	1.1612	1.1701	1.1672	.429
333				
533	1.0672	1.0747	1.0754	.541
200	1.8907	1.9703	1.9700	.165
222	1.8433	1.8885	1.8934	.286
600	1.6469	1.6697	1.6634	.495
244				
622	1.5622	1.5827	1.5866	.547
022	2.2263	2.3401	2.3423	.233
400	2.1938	2.2744	2.2721	.330
422	2.1476	2.2119	2.2020	.404
044	2.0658	2.1204	2.1318	.467
444	1.9484	1.9943	1.9915	.572

BIBLIOGRAPHY

BACON, G.E., Neutron Diffraction, 3rd ed., Oxford [Eng.]: Clarendon Press (1975).

BACON, G.E. and MASON, E.W., Proc. Phys. Soc. 92, 713 (1967).

BACON, G.E. and JUDE, R.J., Z. Kristallogr. 138, 19 (1973).

BEVINGTON, P.R., Data Reduction and Error Analysis for the Physical Sciences, McGraw-Hill (1969).

BIRCHALL, T., RUEBENBAUER, K., and CAMPBELL, C.C.M., Phys. Stat. Sol. (a) 57, 381 (1980).

BIRCHALL, T., RUEBENBAUER, K., and CAMBELL, C.C.M., Phys. Stat. Sol. (a) 59, 347 (1980).

BRADLEY, A.J. and RODGERS, J.W., Proc. R. Soc. Lond. A144, 340 (1934).

CAMPBELL, C.C.M., J. Phys. F: Met. Phys. 5, 1931 (1975).

CAMPBELL, C.C.M. and STAGER, C.V., Can. J. Phys. 54, 2197 (1976).

COOPER, M.J., Thermal Neutron Diffraction, Willis, B.T.M. ed., Oxford Uni. Press. 51 (1970).

COOPER, M.J. and ROUSE, K.D., Acta Cryst. A26, 214 (1970).

COOPER, M.J., ROUSE, K.D., and WILLIS, B.T.M., Acta Cryst. A24, 484 (1968).

COOPER, M.J. and ROUSE, K.D., Acta Cryst. A27, 622 (1971).

FELCHER, G.P., CABLE, J.W., and WILKINSON, M.K., J. Phys. Chem. Solids 24, 1663 (1963).

GARRETT, J.D., GREEDAN, J.E., LOCKE, K.E., and STAGER, C.V., J. Crystal Growth 46, 463 (1979).

HEUSLER, F., STARCK, W., and HAUPT, E., Verh. der deut. phys. Gesell. 5, 220 (1903).

ISHIKAWA, Y. and NODA, Y., Solid St. Comm. 15, 833 (1974).

ISHIKAWA, Y., TAJIMA, K. and RADHAKRISHNA, P.J., J. Phys. Soc. Japan 40, 1597 (1976).

LOCKE, K.E., Master's Thesis, McMaster Uni., (1977), unpublished.

LOCKE, K.E., STAGER, C.V., and BUYERS, W.J.L., Phys. Rev. B23, 5928 (1981).

MARSHALL, W., and LOVESEY, S.W., Theory of Thermal Neutron Scattering, Oxford Uni. Press. (1971).

NODA, Y. and ISHIKAWA, Y., J. Phys. Soc. Japan 40, 690 (1976).

NODA, Y. and ISHIKAWA, Y., J. Phys. Soc. Japan 40, 699 (1976).

NODA, Y., TAJIMA, K., ISHIKAWA, Y., WEBSTER, P.J., STRINGFELLOW, M.W., TOCCHETTI, D., and ZIEBECK, K.R.A., J. Phys. Soc. Japan 43, 483 (1977).

PERSSON, E., Naturwiss. 16, 613 (1928).

POTTER, H.H., Proc. Phys. Soc. 41, 135 (1929).

PRICE, D.C., J. Phys. F: Met. Phys. 8, 933 (1978).

ROUSE, K.D., COOPER, M.J., YORK, E.J., and CHAKERA, A., Acta Cryst. A26, 682 (1970).

ROWE, J.M., Neutron Spectroscopy: The Design and Construction of a Triple Axis Crystal Spectrometer, and a Study of the Lattice Dynamics of Metals, Ph.D. Thesis, McMaster Uni. (1966).

SOBCZAK, R., Solid St. Comm. 29, 451 (1979).

STEARNS, M.B., J. Appl. Phys. 50, 2060 (1979).

WEBSTER, P.J., Contemp. Phys. 10, 559 (1969).

WEBSTER, P.J., J. Phys. Chem. Solids 32, 1221 (1971).

WEBSTER, P.J., J. Appl. Phys. 52, 2040 (1981).

WEBSTER, P.J., and TEBBLE, R.S., J. Appl. Phys. 39, 471 (1968).

WEBSTER, P.J., and TEBBLE' R.S., Phil. Mag. 16, 347 (1967).

ZACHARIESEN W.H., Acta Cryst. 23, 558 (1967).

END

1001184

FIN